UNIVERSITÀ
DEGLI STUDI
DI PADOVA

DIPARTIMENTO
DI INGEGNERIA
DELL'INFORMAZIONE

DEPARTMENT OF INFORMATION ENGINEERING

MASTER COURSE IN
REHABILITATION BIOMEDICAL ENGINEERING

Analysis of EEG Signals for the Detection of Erroneous Commands During the Control of a Powered Wheelchair

Supervisor
Prof. Luca Tonin

Student
Michela Cattabriga

ACADEMIC YEAR 2022-2023

Graduation Date 14/12/2023

Abstract

Error Potentials (ErrPs) are neurophysiological signals generated by users when they perceive errors in their actions and during interaction with brain-computer interfaces (BCIs), following an incorrect response of the BCI. This work focuses on identifying and detecting ErrP signals during the discrete control of a powered wheelchair. Nine healthy subjects voluntarily participated in the experiment. Electroencephalogram (EEG) signals were acquired from the subjects while they controlled the powered wheelchair using a joystick along a predefined path. Random errors were intentionally introduced during the control sessions to elicit ErrP responses.

The EEG signals were analyzed to identify, to characterize the ErrPs, and ultimately to construct a classifier capable of detecting them. The results show a differentiation between the neural responses corresponding to correct and erroneous actions, confirming the presence of distinct ErrP signals following incorrect commands during the discrete control of the wheelchair. A classifier was successfully developed and trained to detect these ErrP signals on a trial-by-trial basis, showcasing promising accuracy in identifying real-time errors.

Furthermore, individual variability in neural activity among subjects was acknowledged, highlighting the necessity for personalized calibration and optimization of system parameters. Future directions involve extending this research to more complex environments without predefined paths to simulate realistic scenarios and testing the system's efficacy with individuals having motor impairments, who are the final end-users.

Sommario

I potenziali di errore (ErrP) sono segnali neurofisiologici generati dagli utenti quando percepiscono errori nelle loro azioni e durante l'interazione con le interfacce cervello-computer (BCI), in seguito a una risposta errata della BCI. Questo lavoro si concentra sull'identificazione e la rilevazione dei segnali ErrP durante il controllo discreto di una sedia a rotelle motorizzata. Nove soggetti sani hanno partecipato volontariamente all'esperimento. I segnali dell'elettroencefalogramma (EEG) dei soggetti sono stati acquisiti mentre controllavano la sedia a rotelle motorizzata utilizzando un joystick lungo un percorso predefinito. Durante le sessioni di controllo sono stati introdotti intenzionalmente errori casuali per suscitare i potenziali di errore.

I segnali EEG sono stati analizzati per identificare e caratterizzare gli ErrP e, infine, costruire un classificatore in grado di rilevarli. I risultati mostrano una differenziazione tra le risposte neurali corrispondenti ad azioni corrette ed errate, confermando la presenza di segnali ErrP distinti in seguito a comandi errati durante il controllo discreto della sedia a rotelle. È stato sviluppato con successo un classificatore in grado di rilevare questi segnali ErrP per ogni comando dato alla sedia a rotella, dimostrando una promettente accuratezza nell'identificazione degli errori in tempo reale.

Inoltre, è stata riconosciuta la variabilità individuale dell'attività neurale tra i soggetti, evidenziando la necessità di una calibrazione soggetto-specifica e dell'ottimizzazione dei parametri del sistema. Le direzioni future prevedono l'estensione di questa ricerca ad ambienti più complessi e privi di percorsi predefiniti, per simulare scenari realistici, e la verifica dell'efficacia del sistema con persone con disabilità motorie, che saranno gli utenti finali.

Contents

List of acronyms

ACC anterior cingulate cortex

ANOVA Analysis of Variance

AUC area under the curve

BCI   Brain-Computer Interface

BMI Brain-Machine Interface

BOLD blood oxygen level-dependent

CAR common average reference

ECoG electrocorticography

EEG   electroencephalography

EOG   electrooculogram

ERP   Event-Related Potential

ErrP   Error-Related Potential

fMRI functional magnetic resonance imaging

fNIRS functional near-infrared spectroscopy

ICA   Independent Component Analysis

LOOCV leave-one-out cross-validation

MEA microelectrode array

MEG magnetoencephalography

MI   motor imagery

ROC receiver operating characteristic

ROS   Robot Operating System

SSVEP steady-state visual evoked potential

Chapter 1

Introduction

A Brain-Computer Interface (BCI), also known as a Brain-Machine Interface (BMI), is a technology that allows the brain to directly communicate with external devices such as prostheses, computers, and robots [1]. BCIs acquire brain signals, analyze and interpret them, and translate them into commands that can be used to control an external device [2]. BCIs have been developed for a variety of purposes, including improving medical care, facilitating communication for people with motor or speech impairments, supporting scientific research, and enabling advanced human-computer interaction [3]. In fact, one of the motivations behind the development of BCIs is the fact that the connection between the central nervous system and limbs might be somehow interrupted caused by various conditions, including brain-related issues like strokes, traumatic brain injuries, spinal cord injuries, or amputations [4]. This loss of communication between the brain and limbs leads to the idea of reestablishing the connection by decoding the user's intentions from neural activity and executing these intentions to control the external device [5] (Figure 1.1). BCIs essentially link the brain's command center directly to software enabling users to train their brain to achieve direct control through thoughts.

These interfaces offer substantial help to people with disabilities in controlling prosthetic devices, or wheelchairs, helping patients recovering from strokes or other neurological disorders, and allowing them to interact with computers or other devices without relying on physical input devices such as keyboards or mice.

1.1 BCI as a closed loop

BCIs are designed as closed-loop systems, delivering real-time feedback to users based on interpreted brain signals [6]. This feedback loop allows users to adapt their brain activity or responses based on visual, auditory, or tactile information provided by the system [7]. Simultaneously, the decoding system, which interprets brain signals, must evolve and improve over time, refining its
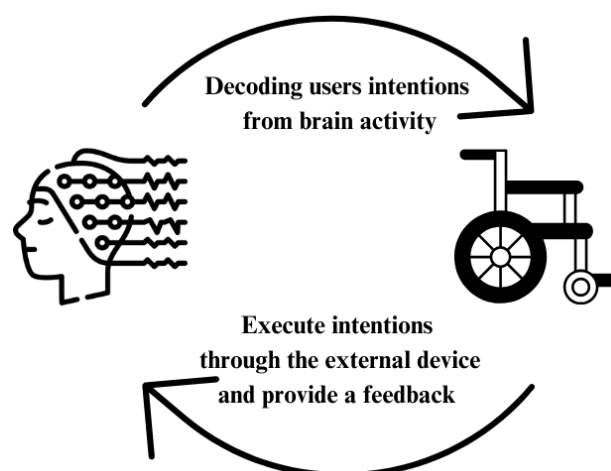
Figure 1.1: *General idea of a BCI*

mathematic models to better match the user's brain activity [8]. This close interaction between the decoder and the user facilitates a process known as mutual learning, where both entities adapt and learn from each other [8].

The functioning of a BCI involves five main steps [1] (Figure 1.2):

1. **Signal acquisition:** The first step of a BCI is the acquisition of brain activity, which can be achieved through various techniques briefly discussed in Section 1.2.

2. **Signal processing:** Acquired signals are processed to facilitate the identification of the most important characteristics of the signals and to facilitate further analysis. This step includes filtering to remove noise, eliminating artifacts, and improving the signal-to-noise ratio [2].

3. **Features extraction:** This step involves extracting important features from the pre-processed signals, such as frequency, amplitude, and phase of the brain waves, used to identify specific mental states or commands [2].

4. **Classification:** Extracted features are used to classify the mental state or command that the user wants to communicate, often employing machine learning algorithms like support vector machines, artificial neural networks, or decision trees [2].

5. **Feedback:** The classified information is used to generate an output that can be used to control an external device. For example, the output can be used to move a cursor on a computer screen, control a robotic arm or a wheelchair, or control a prosthetic limb. The execution of these commands produces feedback, representing the subject's brain activity. The external device enables the user to understand how well they can control the device [2].
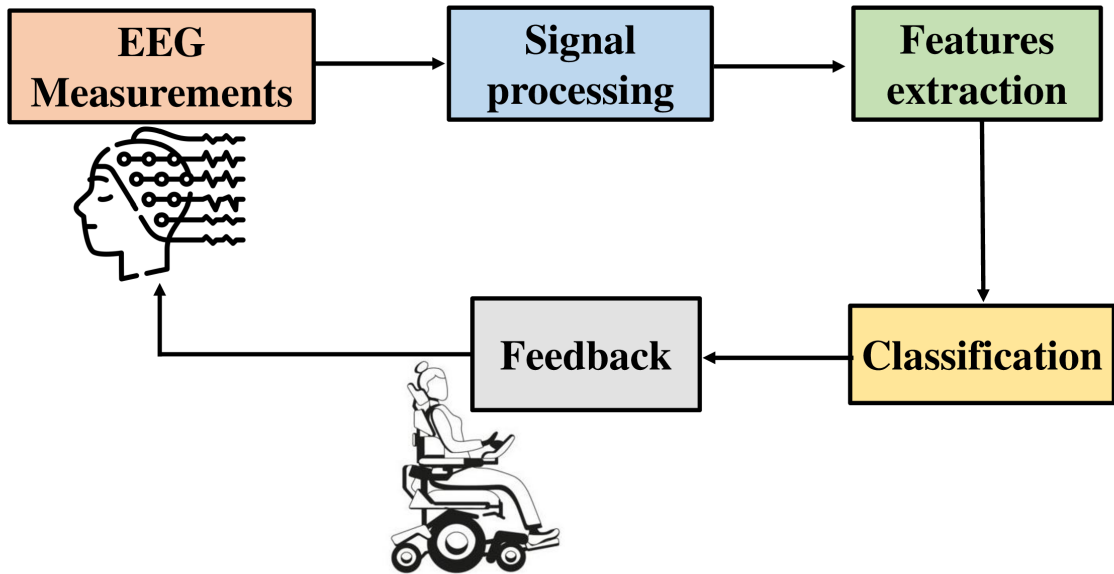
Figure 1.2: *BCI Closed-Loop*

Overall, the success of a BCI depends on the precision and reliability of each stage: acquisition, processing, feature extraction, and signal classification techniques. Each step is fundamental, and even a minor imperfection in any of these phases can make the entire process vanified.

1.2 Invasive and non-invasive BCIs

Understanding user intentions requires recording the brain activity, a process facilitated by various methods that can be divided into invasive and non-invasive techniques [9]. BCIs are therefore classified into two categories based on the acquisition technique: invasive BCIs and non-invasive BCIs [10].

Invasive BCIs record brain activity via surgically implanted electrodes placed close to the target neurons in the cortex [11]. For instance, the microelectrode array (MEA) and electrocorticography (ECoG) electrodes are commonly used [11]. MEA is typically inserted within the cerebral cortex's grey matter, allowing the detection of neuronal action potentials (also known as spikes) generated by single or multiple neurons [11]. ECoG involves direct electrode implantation over the cortex, usually positioned either below or above the dura matter [11]. Remarkably, ECoG was first recorded in humans by Hans Berger in 1929 during a neurosurgical operation on a 17-year-old boy [12]. Invasive electrodes directly placed at the source of brain activity grant significantly higher signal resolution, as the electrical activity originates on the cortex. This provides a superior signal-to-noise ratio and a better localization of brain

activity [13]. However, employing these implanted electrodes necessitates surgical operations, carrying potential risks of scarring, brain infections, and other complications associated with the insertion [14].

On the contrary, non-invasive BCIs collect information about brain activity without surgical procedures using methods such as electroencephalography (EEG), magnetoencephalography (MEG), functional magnetic resonance imaging (fMRI), and functional near-infrared spectroscopy (fNIRS) [11].

fMRI captures blood oxygen level-dependent (BOLD) activity, decoding changes in brain blood flow to offer detailed brain mapping with high spatial resolution [15]. However, its low temporal resolution, due to the timing of oxygenation and deoxygenation of an area of the brain, poses challenges in real-time applications, potentially disrupting closed-loop interactions and impeding user's learning due to feedback delays [16]. Furthermore, its unmanageable size and cost, limit the use of this technique for most BCI applications [13].

fNIRS is an alternative technique that measures BOLD activity [17]. It is a safe, non-invasive, relatively inexpensive, and portable neuroimaging technique that is often integrated with EEG to increase classification performance [18]. However, its low information transfer rate, caused by inherent delays in hemodynamics, remains a limitation [13].

MEG detects the magnetic field associated with electrical brain signals, providing high spatial and temporal resolution [19]. It requires a shielded room and it uses highly sensitive magnetometers (SQUIDs) [20]. However, its impracticality for home use makes it less suitable for BCI applications, even if MEG can capture signals with less distortion and provides a better spatiotemporal resolution compared to EEG [1].

EEG is the most popular non-invasive technique as it is economical, portable, and even compatible with wireless devices [21]. This method measures brain activity through electrodes placed on the scalp. While EEG offers high temporal resolution, detecting events that change in milliseconds, its spatial resolution is limited due to the electrodes' size [13]. Nonetheless, its high usability makes EEG the most common method for non-invasive BCI applications [22]. The resulting brain signals originate from cortical neurons, traveling through several layers before reaching the scalp, producing measurable electrical activity in the brain [1]. Consequently, the signal acquired directly from the brain cortex has a voltage of millivolts (mV), while the signal collected from the scalp, undergoing various layers leading to an attenuation of it, has a reduced voltage of microvolts (μV) [1].

Considering signal frequency, EEG signals are conventionally divided into specific frequency bands: δ (0.5-4 Hz), ϑ (4-8 Hz), α (8-14 Hz), β (14-30 Hz), and γ (over 30 Hz) [23]. These bands represent distinct frequency oscillations associated with different physiological states such as sleep, wakefulness, alertness, and other conditions. Neurologists therefore analyze alterations

in these rhythms compared to normal patterns to diagnose potential diseases [23].

The EEG detects changes in voltage produced by the neuronal activity. When a large group of neurons discharges synchronously, electrical signals are generated and they are detectable on the scalp through the use of electrodes. The voltage changes can be related to responses to internal or external stimuli.

1.3 BCIs based on self-paced activity and evoked potentials

A further classification for EEG-based BCIs is based on the type of brain signal they utilize. EEG signals recorded can be classified as either endogenous (spontaneous) or exogenous (evoked), leading to the categorization of BCIs into self-paced BCIs and evoked potential BCIs [24]. Self-paced BCIs rely on endogenous brain signals, intentionally and spontaneously generated by the user and independent of external stimuli [24]. Users initiate actions or commands voluntarily through their mental processes, like imagining specific movements or intentions. These BCI systems are driven by the intentional motor imagery (MI) of users. MI is a cognitive process in which a subject imagines moving a specific body part without physically performing it [25]. Different studies ([26], [27]) have demonstrated that during both motor execution and motor imagination, there is precise spatial localization in the primary motor area and primary somatosensory area of the brain. This means that imagining a specific body part activates the related area in the motor cortex [28]. Furthermore, MI exhibits spectral localization, with EEG signals oscillating between 8 and 12 Hz [29]. The combination of spatial and spectral localization can be used as crucial features in the development of BCIs based on MI [30].

BCIs based on evoked activity rely on brain signals elicited in response to external stimuli. Exogenous brain signals represent the physiological responses triggered by an external stimulus, typically within the visual, auditory, or somatosensory domains [31]. These stimuli induce measurable brain responses detected through techniques like EEG or fMRI, allowing the interpretation of these signals to understand user's intention [32]. The most common evoked potentials used in BCIs include steady-state visual evoked potentials (SSVEPs), P300, and Error-Related Potentials (ErrPs) [33]. The activities associated with evoked potentials are time and phase-locked, meaning that after each repetition of the stimulus, the evoked potentials always appear with a certain delay and shape [34]. This facilitates the evoked potentials analysis allowing a linear temporal analysis to recognize the shape [34].

SSVEPs are based on visual stimulation, often involving the flickering of an object at a specified frequency on a computer screen [35]. SSVEP BCIs are completely passive with respect to the cognitive state of the subject [35]. They primarily reflect the representation of visual stimuli within the occipital cortex, thereby indicating the subject's visual focus [35]. While this method

works quite well, the fact that it relies on a fixed monitor placed in front of the user can be considered uncomfortable for prolonged use [36].

P300 is a component of the Event-Related Potential (ERP) that is generated after visual or auditory exogenous stimuli [37]. Specifically, it represents a brain response to a rare target stimulus [38]. It is most frequently elicited within a framework called the "oddball paradigm" [38]. In this paradigm, the subject is presented with a sequence of events that can be classified into two categories. In general, events in one of the two categories are rarely presented [38]. Under these circumstances, events in the rare category elicit an ERP characterized by a P300 component [39]. This attention to the target stimulus triggers a cognitive process generating a positive deflection in the EEG signals approximately 300 milliseconds after the rare stimulus presentation [40]. Detection of the P300 typically occurs in the central scalp position (Cz, FCz, Fz electrodes) [41].

The ErrP is a brain response to an erroneous stimulus [42]. This response is widely discussed in the following section (Section 1.4) since it is the focus of this research thesis.

1.4 BCI based on Error-related potentials

ErrP is an evoked potential in response to an incorrect stimulus [42]. It originates from the anterior cingulate cortex (ACC), a deep region situated in the brain [43]. This area plays a crucial role in regulating emotional responses [44]. ErrP is typically detected through electrodes centrally positioned on the scalp, such as Fz, Cz, and predominantly FCz because ErrPs are characterized by a fronto-central distribution along the midline [42]. Different typologies of ErrP have been identified:

- **Response ErrP**: occurs when the subject is asked to respond as quickly as possible to a stimulus, resulting in ErrP following errors arising from incorrect motor actions. The primary components are a negative potential appearing approximately 80 ms after the erroneous response, followed by a larger positive peak occurring between 200 and 500 ms after the incorrect response [42].

- **Feedback ErrP**: arises when the subject is asked to make a choice and ErrP follows the presentation of a stimulus that indicates incorrect performance. The main component is a negative deflection observed around 250 ms after the presentation of the feedback indicating incorrect performance [42].

- **Observation ErrP**: may be present when observing errors made by an operator during a choice reaction task. Similar to feedback ErrP, the main component is a negative potential showing up 250 ms after the operator's incorrect response during the task [42].
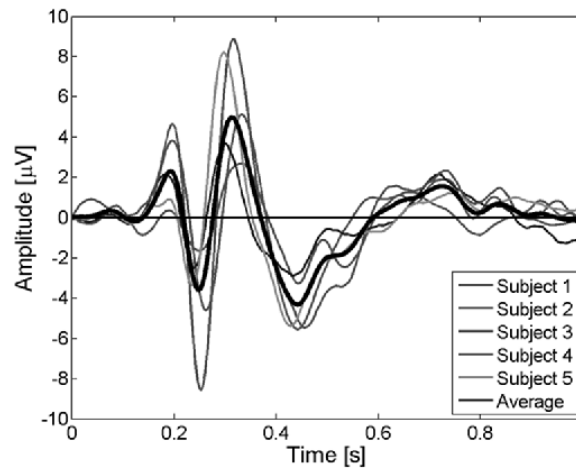
6

Figure 1.3: *Shape of interaction ErrPs. Average EEG for the difference error-minus-correct at channel "FCz". Feedback is delivered at time 0 s. A first positive peak shows up after 200 ms after the feedback. Negative and positive peaks show up about 250 and 320 ms after the feedback, respectively [42]*

.

- **Interaction ErrP**: elicited when, for example, the subject is asked to make a robot reach a target, and an error occurs during the BCI's recognition of the subject's intent, leading the robot to perform the opposite action. In general, it arises whenever the BCI wrongly interprets the user's intention and the user perceives the error. The main components include an initial positive peak around 200 ms after the feedback, followed by negative and positive peaks approximately at 250 ms and 320 ms after the feedback. Finally, a second broader negative peak occurs about 450 ms after the feedback [42]. The pattern of this ErrP is illustrated in Figure 1.3.

It is relevant to note that the latency of the positive and negative deflections within ErrP may vary depending on the specific task demands and context [45].

1.5 Related works

Scientific research has developed several BCI systems based on ErrPs. Since BCIs may misinterpret the subject's intention, ErrP can be useful to correct the actions [46]. ErrP has been employed both in active BCIs and passive BCIs. An active BCI involves the user controlling the external device through MI. In the event of a misinterpreted command, an ErrP is generated. The interface decodes the ErrP to correct the action. Conversely, in a passive BCI, the user monitors actions independently executed by an external device [47].

In an experiment by Chavarriaga and Millán, it was demonstrated that ErrPs arise when a user

monitors the performance of an external robot. In this scenario, the user acts as a critic of an external autonomous system instead of directly controlling the movements of the device. This highlights the possibility of achieving optimal robot behavior in line with the user's intention, allowing for customization of the robot's behavior according to the user's needs and preferences. In this situation, the subject passively monitors the robot's behavior while the robot itself exploits the ErrP as feedback to achieve the goal [48].

Ferrez and Millán conducted an experiment demonstrating the existence of ErrP resulting from a failure of the BCI to execute a command. Participants were asked to bring a cursor to a target position on a computer screen. To prevent ErrP recognition caused by the classifier's failure to interpret the user's MI, commands were manually, rather than mentally, sent by the user. This approach aimed to attribute any error feedback only to incorrect implementation of the commands by the interface. Introducing a 20% probability, the system moves the cursor in the opposite direction compared to the user's intended movement, thereby inducing an ErrP. This study shows the occurrence of ErrP as a result of a misinterpreted action by the BCI [42].

The same experiment was conducted with commands delivered by the user through MI instead of manually. In particular, this experiment demonstrated the simultaneous detection of interface errors and real-time MI classification. Users were asked to mentally control the movement of a cursor toward a target. One classifier interpreted and executed the command, while simultaneously another classifier analyzed the user's brain signals after the command was executed, assessing the presence of the ErrP and, if detected, correcting the action performed on the cursor. This research demonstrates the possibility of simultaneously extracting useful information for the control of external devices via MI, while evaluating the brain response following the action, thus improving the performance of the BCI [49].

In recent years, among various BCI applications, the use of the human brain in wheelchair movement and control has gained attention in the scientific community due to its potential to help elderly and paralyzed individuals, potentially improving their independence and quality of life. EEG-based wheelchair systems use EEG data from the human brain for system control. Researchers have demonstrated the feasibility of controlling wheelchairs through MI [50]. Tsui et al. presented a self-paced MI-based BCI enabling the user to fully control the wheelchair [51]. In a study by Li et al. [52], an EEG-based wheelchair was designed, allowing users to steer the wheelchair using only their thoughts without any other involvement, showing a potential practical application for disabled people. Tonin et al. demonstrated the successful training of individuals with tetraplegic spinal cord injury to operate a non-invasive, self-paced controlled wheelchair, enabling them to perform complex navigation tasks [53]. This study explores the feasibility of achieving continuous wheelchair control using MI [53].

However, MI BCIs might misclassify the user's intention, resulting in incorrect wheelchair

movements. To address this, an idea is to implement a classifier alongside the MI BCI that detects ErrPs. Upon detection, the wheelchair's action could be corrected.

1.6 Objectives and motivations of the thesis

Several scientific studies have demonstrated the feasibility of controlling wheelchairs using brain signals [50]. However, current BCIs are not entirely reliable in accurately detecting user intention and they may wrongly recognize the subject's intent. This lack of precision—partly due to the variability of brain signals between individuals [50]—can lead to incorrect interpretation of commands given to the wheelchair. As a result, BCI-based wheelchair control does not currently provide full autonomy and safety in a real-world scenario [50].

To ensure safe and efficient control, it is crucial to develop a system that not only interprets brain signals for wheelchair control (e.g., go straight, go left, or go right), but is also able to detect and correct the wrongly interpreted intention of the user. The aim is to implement an algorithm that assesses the brain's response when the interpreted intention is translated into a command executed by the wheelchair: if the intention is wrongly decoded, the user will generate a detectable ErrP that can be used to correct the action. As shown, a system of this type has already been implemented in stationary conditions. Currently, this methodology has not been developed during operation with wheelchairs. Therefore, the aim of this research is to investigate the feasibility of decoding ErrP and correct eventual errors during wheelchair operations. To simplify the protocol, the user's will not mentally control the wheelchair via BCI but manually through a joystick. Therefore, the primary objective of the thesis is to determine the presence of ErrPs during wheelchair control using a joystick, identify and classify them with an offline analysis, and establish a baseline for the potential development of a corrective algorithm to use during the real-time control of a wheelchair. Future work will involve the integration of this protocol with MI BCI in order to increase the effectiveness control of the device.

Chapter 2

Materials and Methods

This experiment aims to investigate, identify, and classify ErrPs through EEG signals. In this chapter, the experimental protocol, participant selection, the equipment, the experiment's setup, and data analysis methods are reported.

2.1 Participants

Nine able-bodied, healthy subjects (7 males and 2 females) between the ages of 22 and 26 voluntarily participated in the study. Participants were carefully selected to ensure a homogenous and healthy cohort. Inclusion criteria involved the absence of chronic medical conditions, such as neurological disorders, and any ongoing conditions that might potentially influence the results of the study. This rigorous selection process was designed to provide a consistent and uniform baseline, enabling a more focused investigation of the variables under study and ensuring a more robust and reliable analysis of the experimental outcomes. Written informed consent was given to all participants before taking part in the study, explaining all the details of the experiment and how the recorded data would be used afterward. Each participant completed the experiment in a single session lasting approximately two hours.

2.2 Materials

2.2.1 Powered Wheelchair

A customized powered wheelchair (Figure 2.1) has been employed in this study. The powered wheelchair was transformed into an intelligent robot through the integration of multiple sensors such as RGB cameras, LiDARs, and encoders [54]. For this experiment, a commercial wheelchair has been modified and it has been connected to a gamepad controller. The

Figure 2.1: *The powered wheelchair employed in the experiments*

wheelchair's movement was enabled by individually driven front wheels, while the passive castor rear wheels provided frame support. Additionally, a laptop computer, positioned at the rear during the experiments, recorded all the essential data required for the subsequent analysis.

2.2.2 Joypad

Even if the wheelchair has a built-in joystick, in the study under analysis an external joystick was used to control its movement. Specifically, the gamepad utilized was a "Logitech F710 wireless gamepad" (Figure 2.2). The control through the joystick offered both a continuous and a discrete mode for the control. Continuous control allowed the user to navigate the wheelchair using the analog stick, while discrete control necessitated the use of buttons. Although both controls have been implemented during the experiments, this thesis focuses on the discrete control. Further details are given in Section 2.4.

2.2.3 EEG cap

Since the experiments required the acquisition of subjects' brain signals, the use of an EEG cap was necessary. In particular, an ANT Neuro EEG cap, eego^{tm}sports, with 64 electrodes was used to collect the EEG data (Figure 2.3). The main advantage of this EEG cap is that it has shielded

Figure 2.2: Joypad: *Logitech F710 wireless gamepad used in the experiments.*

Figure 2.3: EEG cap: *ANT Neuro EEG cap used for the EEG acquisition.*

cables and a battery-powered amplifier that can be used in a wheelchair. Another advantage of this cap is that the electrodes are pre-positioned according to the international standard 10/20 system. The international 10/20 placement system is a particular scheme for placing electrodes on the scalp [55]. It considers two landmarks on the head: the Nasion, which is the depressed area between the eyes just above the bridge of the nose, and the Inion, which is the crest point of the back of the skull [55]. The electrodes are placed at intervals of 10% or 20% of the distance between these landmarks [56]. This montage setting allows to reduce the time for preparing each participant for the experiment [57]. During the research, not all 64 electrodes were exploited but only 32 electrodes: FP1, F1, FC5, FC3, FC1, C1, C3, C5, CP5, CP3, CP1, P1, P1, P3, P5, Pz, FP2, Fz, F2, FC6, FC4, FC2, FCz, Cz, C2, C4, C6, CP6, CP4, CP2, P2, P4, P6. The reason

behind this choice is the fact that the excluded electrodes are placed over areas of the brain that are not of interest for the study in analysis, and so to reduce the preparation time, half of the electrodes were not considered. In addition, the electrooculogram (EOG) electrode is placed under the participant's left eye to detect eye movements. After the cap has been placed upon the participant, it was of crucial importance to verify that the electrodes were correctly positioned [58]. This was done by identifying the midpoint between the Nasion and the Inion, as well as the midpoint between the two preauricular points. The electrode labeled Cz must be precisely located at the intersection point of these identified landmarks. This electrode placement procedure ensured accurate and reliable data acquisition [57]. Afterward, to obtain a stable electrical connection between the electrodes and the scalp, and thus a clean EEG signal, it was important to have a low impedance so that the signals were not distorted [59]. To achieve this, a gel was applied to each electrode.

2.3 Robot Operating System - ROS

The various components communicate through the Robot Operating System (ROS) middleware. ROS is a distributed framework of processes that enables executables to be individually designed and loosely coupled at runtime [60]. In particular, ROS-Neuro was exploited, which is an open-source framework for neurorobotic applications based on ROS [61]. The ROS processes are depicted as 'nodes' within a graph structure, interconnected by 'topics'. To easily launch multiple ROS nodes, `roslaunch` is employed [62]. `roslaunch` is a tool that accepts a `.launch` file specifying parameters to set and the nodes to launch [63]. In this experiment, a single launch file was created, detailing all necessary nodes that need to be executed. In particular, the following nodes were necessary:

- a node needed for the acquisition of the EEG signals

- a node required to save the EEG data in `.gdf` files

- a `joy` node used to handle the commands that come from the joystick

- a customized node used to manage the communication between the joystick and the wheelchair, which is discussed in the Subsection 2.4.1.

- a record node that uses the `rosbag` package to record all data into bags file (`.bag` extension). Those files contain the data about the wheel odometry and velocities of the wheelchair.
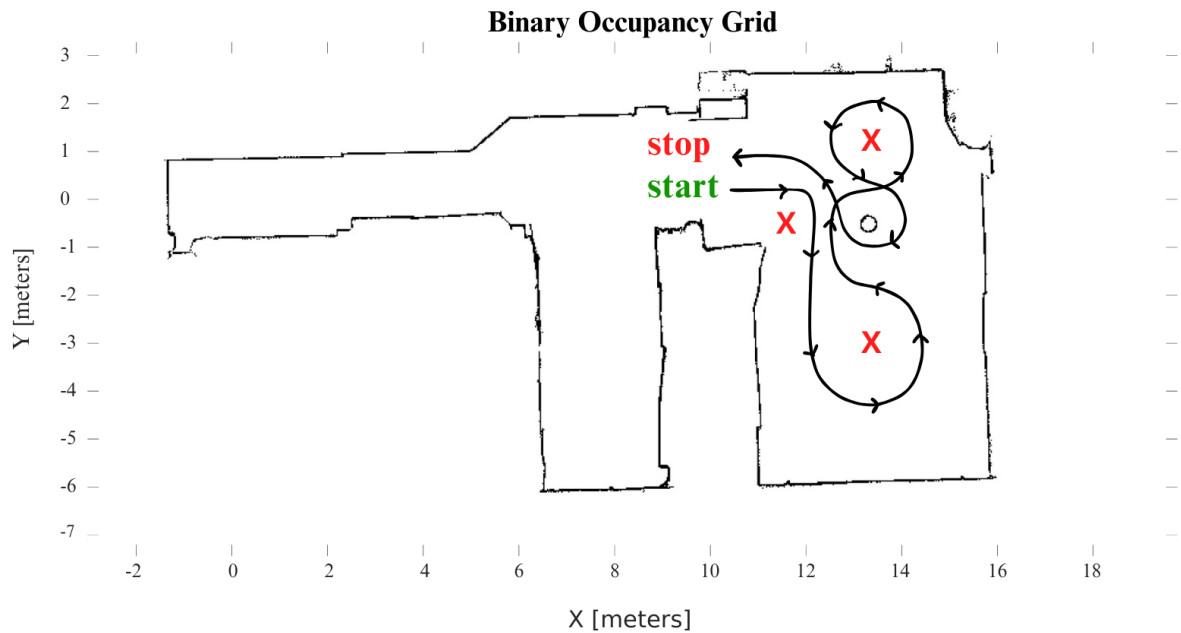
Figure 2.4: *Path the users had to follow while driving the wheelchair. The red crosses represent the static obstacles to be avoided*

2.4 Experiment Description

The research, as already highlighted, consisted of driving the wheelchair using a joystick and analyzing the EEG signals. Therefore, during the experiment, participants sat in the wheelchair while the operator fit the EEG cap and provided the instructions on the experimental procedures. Simultaneously two different research experiments were carried out: the discrete control, where the user controlled the wheelchair using the buttons, and the continuous control, allowing the wheelchair navigation via the analog stick. Throughout the experiment, participants were asked to drive the wheelchair along a predefined path. We refer to each repetition of the path as a "run" and the maximum duration of it was defined as 240 seconds. The total number of runs was 16, including 8 runs each for discrete and continuous control. Additionally, two preliminary test runs were conducted—one for each control type—to allow the users to understand the control mechanisms. The path, as shown in Figure 2.4, was designed to induce the users to make as many turns as possible, avoiding static obstacles defined by chairs.

Since the thesis focuses on discrete control, only the description of this is reported below. The possible buttons the user could use and the resulting actions on the wheelchair are the following:

- **START** (A) button: upon pressing this button (the green button in Figure 2.2), the wheelchair took a fixed and constant linear velocity.

15

- **STOP** (B) button: upon pressing this button (the red button in Figure 2.2), the wheelchair stopped moving and both the linear and angular velocities were set to zero.

- **LEFT** (L1) and **RIGHT** (R1) buttons: these buttons (the circled buttons in Figure 2.2) provided fixed rotations to the left or the right. The fixed rotation was approximately 75 degrees. The rotation lasted for 1.5 seconds, after which the angular velocity was set to zero. In the next 3 seconds after a turn command is delivered, users cannot control the movement of the device.

The customized algorithm used to control the wheelchair interpreted the joystick inputs and translated them into the actual wheelchair movements. To induce potential errors in participants, with a certain probability the turning command given by the user might be reversed, causing the wheelchair to execute the opposite rotation. Furthermore, participants were also instructed to fix a cross in front of them to reduce eye movements and blinking as much as possible, and not to talk or move during individual runs as these could cause artifacts in the EEG signals.

2.4.1 Customized control algorithm

To handle the communication between the joystick and the wheelchair via a custom ROS node, a control algorithm in Python was created. This node was responsible for translating joystick commands into wheelchair motion commands by publishing them to the `cmd_vel` topic, and publishing events related to the joystick buttons pressed to the `events/bus` topic. Each event was defined by a code shown in Table 2.1, useful for later analysis. At the beginning, the code randomly generates a number of errors between 1 and 4 that will be present in the run. The decision of this range of errors was designed to prevent errors from occurring one after the other and to prevent the total number of errors during the experiment from being too high. In this way, the user does not get used to errors and can still perceive them as such. afterward, the duration of a run is divided into N windows, where N is the duration of the run divided by the number of errors, and for each window, the time at which an error will be induced was randomly generated. Each time a command was received from the joystick, the code analyzed the type of command and managed the chair's behavior according to various conditions. If the "start" command was activated, the chair began to move at a constant linear velocity for the entire duration of the run, unless a "stop" command was received, in which case the chair stopped immediately by resetting the linear and angular velocity to zero. For "left" and "right" commands, if a command was detected within a 3-second interval from the previous command, the code only published the events related to the unreleased command without actually sending velocity commands to the chair (Figure 2.5). On the other hand, if the time elapsed since the last command was longer than 3 seconds, the code checked whether or not an error should be generated: if the error has

Table 2.1: *Codes related to the events of the buttons pressed on the joystick. Error mask and No released mask are summed to the event related to the button pressed when necessary*

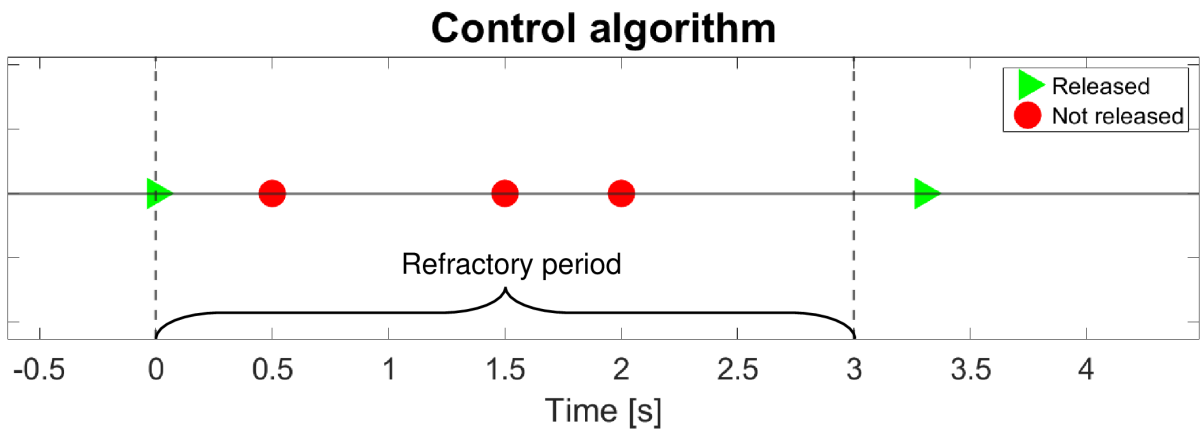| COMMAND	EVENT
FORWARD	102
LEFT	101
RIGHT	103
STOP	100
ERROR MASK	5000
NO RELEASED MASK	4000

Figure 2.5: Control algorithm: *The graph explains the control algorithm. At time 0 a command is released (green triangle). Between 0 and 3 seconds, every command sent by the user is unreleased (red circle). After 3 seconds from the first released command, another command can be released.*

not been generated yet and the time elapsed within the time window exceeded the predetermined instant for the error, the code sent an error command to the chair. Otherwise, if the error had already been generated, the code converted the received command into a correct command to be sent to the chair. It is useful to remember that only left and right commands can be reversed.

2.5 Data analysis

2.5.1 Filtering and artifacts removal

EEG signals were acquired using the ANT Neuro EEG cap with a sampling rate of 512 Hz. In general EEG signal suffers from spatial blur due to the superposition of neural sources across a broad cortical area, leading to neighboring electrodes capturing mixed signals influenced by nearby neuronal activities [64]. To address this challenge, spatial filtering is a common tech-

nique used to reduce this issue and emphasize local neural components [65]. First of all, an initial separation of EOG signal from the other raw signals acquired by the 32 electrodes was needed to prevent eye-movement components and blinks from being introduced into the signals of interest during subsequent filtering. Among different spatial filters, the common average reference (CAR) filter is a widely used technique in EEG pre-processing. Therefore, raw EEG data were first spatially filtered with this technique. This filtering method aims to reduce the common activity among all the electrodes by subtracting the average potential of all the electrodes from each electrode's potential [66]. Doing so helps highlight local variations by minimizing the shared activity across electrodes [66], [67]. Then, we applied a 1-45 Hz bandpass filter to remove the noise and used the Independent Component Analysis (ICA) to try to clean the data from the artifacts, such as eye blink, electrocardiogram, and electromyogram artifacts [68], [69]. Since the focus is on ErrPs (slow cortical potentials), the clean dataset was band-pass filtered at 1-8 Hz with a casual 4th order Butterworth filter [42], [70]–[72]. Since ICA cannot be applied online while CAR filtering can, we wanted to determine whether or not the removal of eye artifacts via ICA was necessary. Therefore we wanted to understand whether or not the filtered signals with and without the removal of some of the independent components were similar enough to avoid ICA, thus be able to apply the protocol online and in real-time. By calculating the cross-correlation between the signals and the EOG, it is possible to determine how similar EEG signals are to the EOG. This allowed an assessment to be made of whether the removal of artifacts by ICA makes a significant difference to the EEG signals compared to the simple application of CAR. If the signals filtered with and without the use of ICA show considerable similarity, then one could avoid using ICA and only apply the CAR filter. This allowed us to simplify the process without compromising the quality of the signals, making it more suitable for online and real-time implementation. The similarity between EEG signals without applying CAR filter, EEG signals with CAR applied, and EEG signals with both CAR and ICA applied, only for the significant channel FCz, versus EOG was calculated. In addition, to provide a more robust and reliable measure of the significance of the cross-correlation results obtained, statistical tests were performed on the cross-correlation results at zero lag—i.e., when the two signals were perfectly overlapped. Statistical tests allow us to determine whether the similarity measures obtained are statistically significant or whether they are due to chance or noise. Specifically, in this case, an Analysis of Variance (ANOVA) test with Bonferroni correction was used to assess the significance of the results. One-way ANOVA tests the hypothesis that the different groups come from populations with the same mean against the alternative hypothesis that the population means are not all the same [73].

2.5.2 Trials extraction

As the analysis in this research focuses on the brain response following a turn, a restricted time window of data associated with each turn command was extracted from the filtered signals. Specifically, a window of 3 seconds was extracted, starting 1 second before the command release and ending 2 seconds later. We defined this time interval as a 'trial'. This approach makes it possible to focus exclusively on the critical period in which the brain response could be influenced by the wheelchair rotation, thus contributing to a better understanding of how the brain reacts during this process. The trials were divided into two distinct classes: 'correct trials' and 'incorrect trials'. Correct trials were associated with correctly executed commands from the wheelchair, where the wheelchair correctly follows the command given by the user. These trials represented the expected response to the user's request. On the other hand, incorrect trials referred to commands that were reversed by the wheelchair—i.e., when the chair did not correctly execute the user's command. Dividing the trials into these two classes makes it possible to study in detail the differences in brain responses associated with correct and incorrect executions.

2.5.3 Delay computation

It is proved that wheel movement sometimes suffers from uncertainties caused by wheel slip and drift [54]. Consequently, an important consideration arises from the delay in the wheelchair movement. It was essential to assess the participants' awareness regarding the actual execution of commands after delivering them. Delays in command execution may be due to both technical and design aspects of the wheelchair, which may influence the movement, as well as individual parameters of the participants, such as the user's weight or the way the user drove the device and the position of the wheels at the time the button was pressed. This analysis was important in order to understand when participants realized the command execution and perceived a possible error. To account for this delay, an approach exploiting the angular velocity was utilized: upon a user command, the wheelchair's angular velocity and the time instant were noted. We hypothesized that the moment when the user actually perceives the rotation was strictly dependent to the angular velocity of the wheelchair. Therefore, for each left and right turn commands, we considered the instant when the angular velocity exceeded a subject-specific threshold (depicted as dashed black lines in Figure 2.6). Finally, we computed the difference between when the command was delivered and when it was effectively perceived by the participant (blue dots and the red dots in Figure 2.6).

Once the delay was applied to each trial, the averages along the trials for the two classes were computed separately. A visual inspection of the averages was carried out to assess if there were any qualitative differences in the brain responses among the different channels.
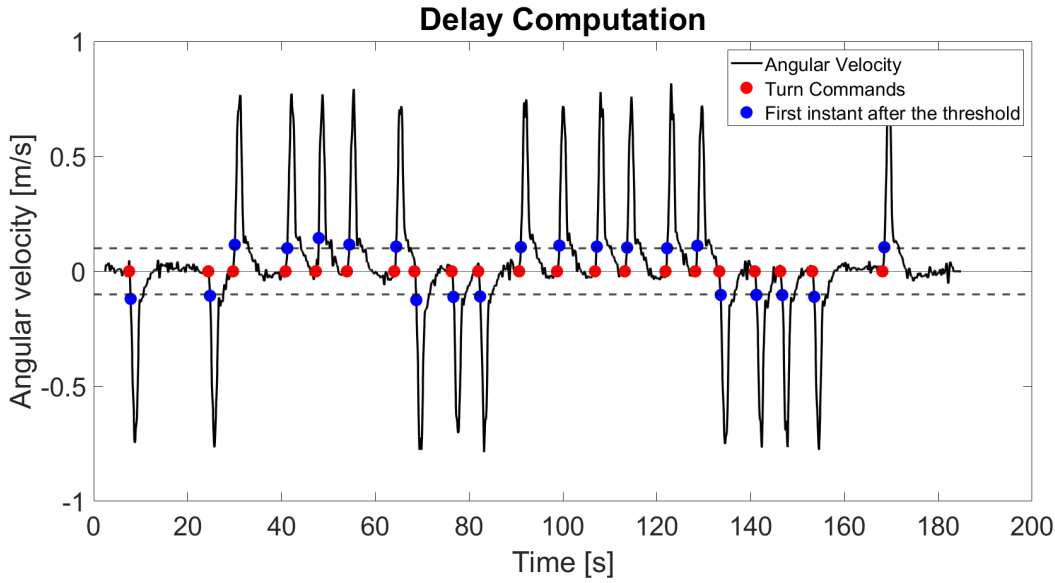
Figure 2.6: *Delay computation: The angular velocity is depicted by the black line. Red points indicate turn commands. Subject-specific thresholds are represented by black dashed lines. Blue dots mark the first time point after the threshold. The delay for each trial is calculated as the difference between the timing of the blue and red dots.*

2.5.4 Classification

As suggested in the literature [42], [70], [71], after data processing, the EEG signals were down-sampled from 512 Hz to 64 Hz before the classification, which was based exclusively on temporal features. The start of the time window for each trial was determined as follows: the time at which the joystick button was pressed was taken into account. The specific delay value for each trial was added to this initial time. This procedure made it possible to define the starting point of the time window used for the analysis of the EEG signals. The length of the time window selected for the classification was 0.7 seconds. The input features vector size for classification is determined by the number of trials times the number of samples corresponding to 0.7 seconds (45 samples) multiplied by the number of the selected channels that vary from subject to subject. It is important to note that the reference channels used for the analysis varied from subject to subject and were selected according to visual inspection. The feature matrix was then divided into training and test sets as follows: the first 70% of the trials were included in the training set, and the remaining data defined the test set. The model used to detect the two different classes (correct and incorrect trials) was a Naive Bayes model [74]. This model was trained on the training set and then tested on both sets (training and test) to assess its ability to correctly discriminate between the two classes. The classifier's performance was assessed by comparing the model's predictions with the true values and computing accuracy, specificity, and sensitivity rates. These recognition rates can be evaluated from the confusion matrix, indicating the num-

20

Table 2.2: Confusion Matrix: *TP refers to true positive; FP refers to false positive; FN refers to false negative; TN refers to true negative; in this specific case 0 is the label for the correct trials and 1 is the label for error trials.*

		Predicted Value	
		Positive	**Negative**
True Value	**Positive**	TP	FN
	Negative	FP	TN

ber of correct and incorrect predictions for each class - the positive class refers to *correct trials* and the negative class refers to *error trials* (Table 2.2). The calculation of recognition rates is expressed as follows:

$$\text{Accuracy} = \frac{TP + TN}{TP + TN + FP + FN}$$

$$\text{Specificity} = \frac{TN}{TN + FP}$$

$$\text{Sensitivity} = \frac{TP}{TP + FN}$$

Due to data imbalance (more correct trials than incorrect ones), high accuracy values might be achieved even if incorrect trials were misclassified. To address this, the true positive rate and the true negative rate were used to generate the receiver operating characteristic (ROC) curve [75]. The ROC curve visualizes the model's performance, where the x-axis represents the false positive rate (1 - specificity), and the y-axis denotes the true positive rate [75]. Furthermore, the area under the curve (AUC) summarizes the ROC curve as an index to assess the classifier's effectiveness in distinguishing classes [75]. An ideal classifier exhibits high sensitivity, high specificity, and yields an AUC of 1, reflected in the ROC curve deviating significantly from the diagonal and ideally intersecting the point (1,0) [75]. Consequently, an AUC value of 1 indicates a perfect classifier, characterized by 100% sensitivity and specificity. In general, the closer the apex of the curve is to the upper left corner, the better the discriminatory ability of the test (i.e., higher true positive rate and lower false positive rate) [76].

As the future goal is the online identification of ErrPs, a sliding window classification was also performed. In this situation, the length of the extracted trials was 1.2 seconds from the moment the button was pressed. Each trial was divided into 33 overlapping sub-windows, with each window shifted by one sample relative to the previous one. The previously trained classifier

was used to classify each sub-window. To assign a unique result to each trial, a subject-specific metric based on the posterior probabilities was developed: if the number of windows with posterior probabilities above a threshold exceeded a certain value, the trial was considered incorrect; otherwise, it was classified as correct.

Chapter 3

Results

This chapter presents in detail the results of the analysis carried out, providing a comprehensive overview of the research outcomes.

3.1 Delay analysis

As explained in Section 2, a crucial aspect of this study involves evaluating participants' awareness regarding the temporal gap between command delivery and actual execution by the device. This analysis is helpful in order to hypothesize when participants realize the command execution and perceive a possible error. Figure 3.1 displays the mean delay values record for each individual subject. This visualization offers an overview of the observed delays showing the variations and average delay times across the different participants.
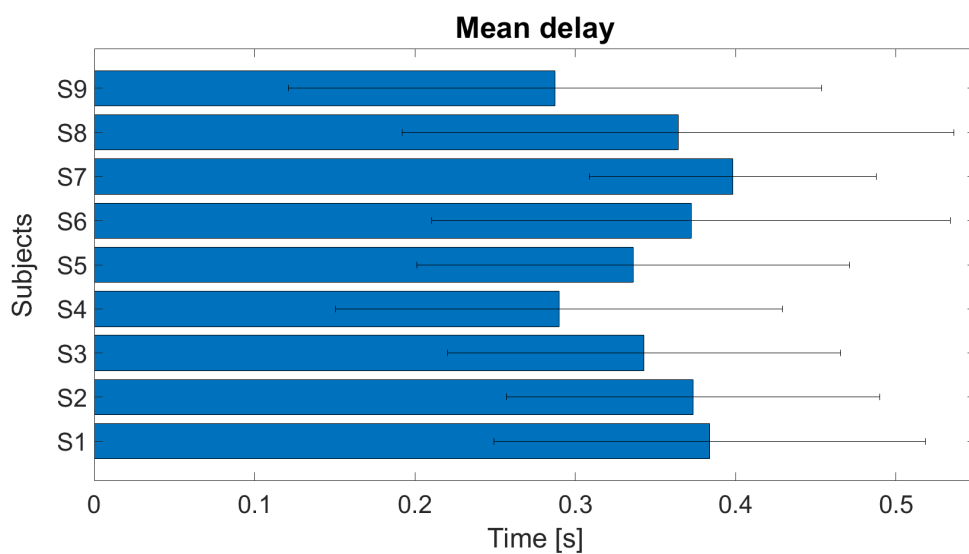
Figure 3.1: Mean delay: *The mean values of the delay for each of the nine subjects. The black lines represent the standard deviation.*

3.2 Grand-Average analysis

Firstly, it was essential for this research to examine the presence of ErrP by analyzing the brain responses following the execution of a wrong action by the wheelchair. Figure 3.2 shows the grand average brain responses for all the nine subjects recorded during error trials with the standard error denoted by the red curve, and the average responses during correct trials with the standard error depicted by the blue curve for channel FCz. Additionally, the difference between the average of the error trials and the average of the correct trials, labeled as error-minus-correct, is presented as the black curve. Figure 3.2 also depicts the topoplots of error and correct trials at the time points 0.1738, 0.373, and 0.634 seconds.
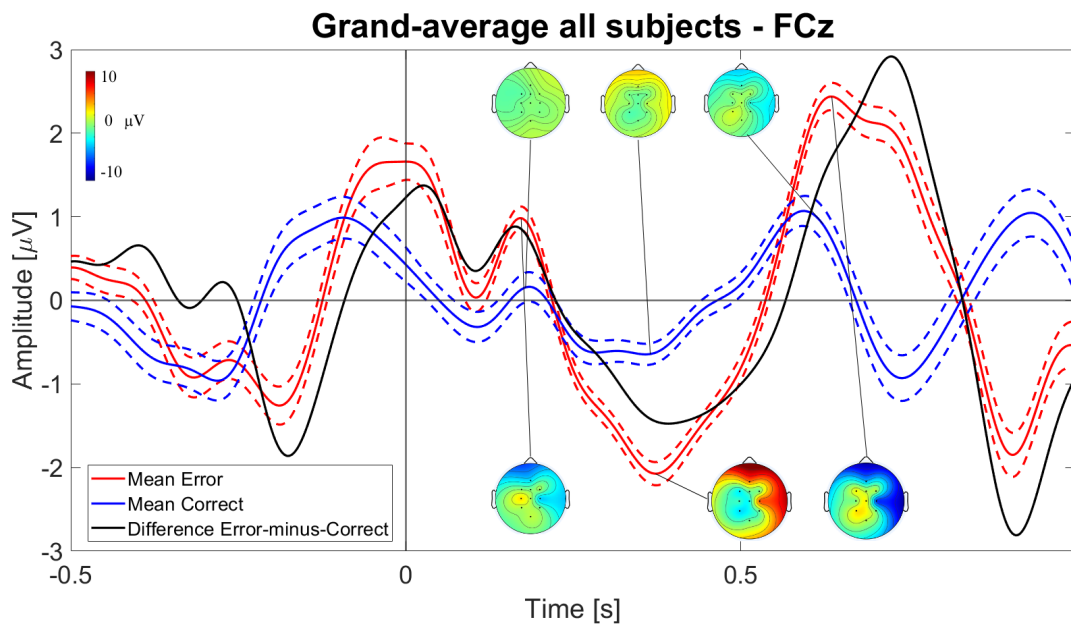
Figure 3.2: Grand-average: *Grand-average of error (red curve) and correct (blue curve) trials with the standard error (dotted lines) at channel FCz. From the grand-average S2 was excluded. The vertical line at time 0 seconds represents the instant the user perceives the error. The upper topoplots are related to correct trials. The lower topoplots are related to error trials.*

After a visual inspection of the overall subjects' responses, a subject-specific analysis was carried out. The brain activity for the nine subjects was analyzed across four distinct channels: 'Fz', 'Cz', 'Pz', and 'FCz' selected for their relevance in capturing ErrP signals. Hereafter, the average correct (blue curve) and error (red curve) signals with the standard error at channel FCz for two different subjects are depicted in Figure 3.3 and Figure 3.4. In particular, S4 shows good results, reporting a different brain behavior for error and correct trials. Conversely, the results of S2 show little variation between the two classes leading to a more difficult analysis and classification. All the other results are reported in Appendix A. The curves from the 9 subjects enable visualization and comparative analysis among them and the two different classes.
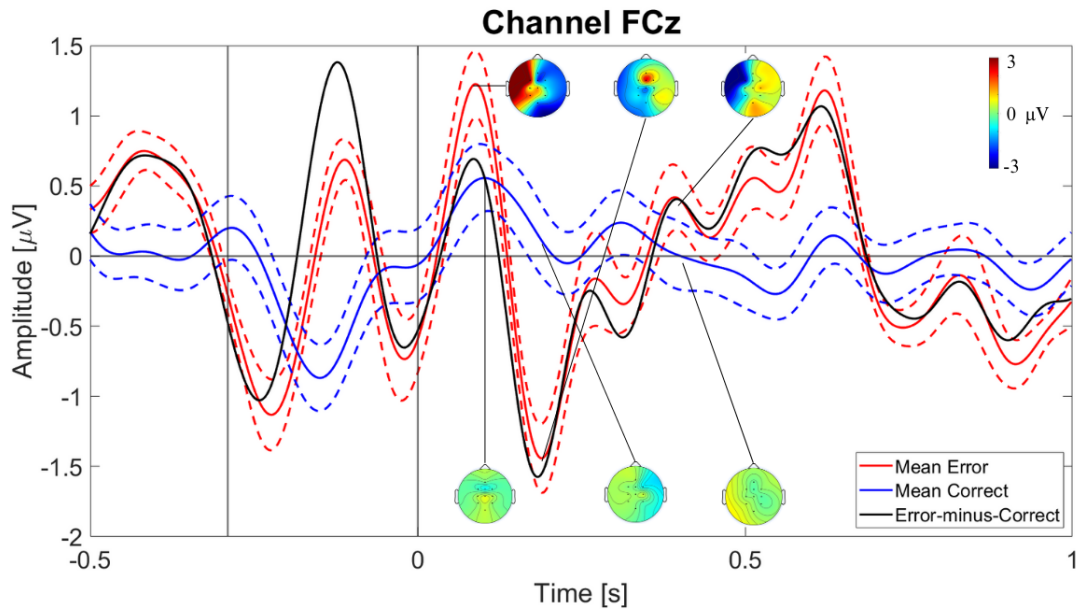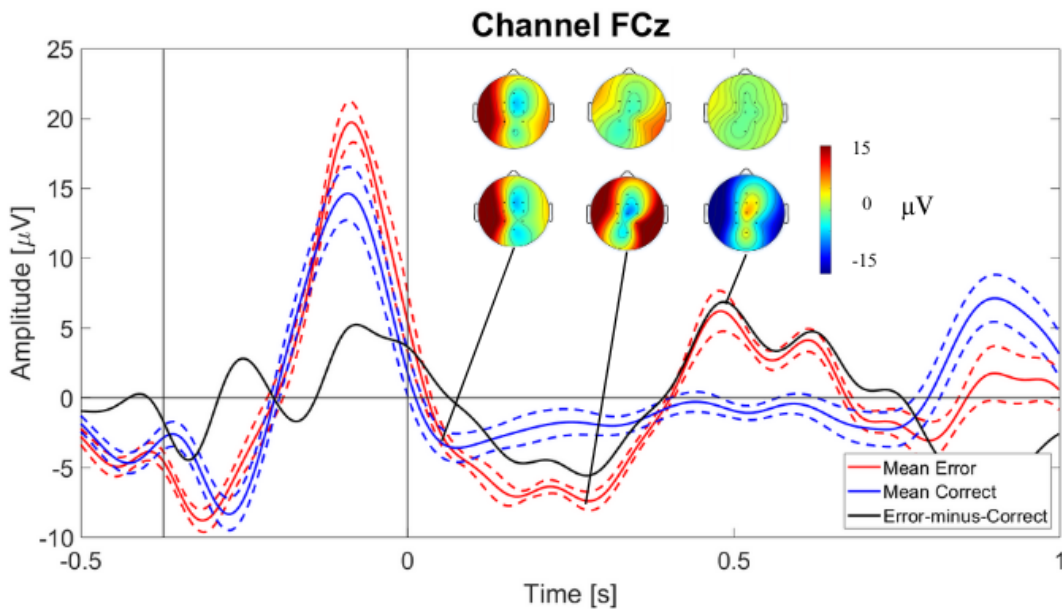
Figure 3.3: Grand-Average S4: *Averages of error trials (red curves), of correct trials (blue curves), and the difference error-minus-correct (black curves) for **S4** for channel FCz. The dotted lines depict the standard errors. The first vertical line represents, on average, the command onset. The vertical zero line represents the instant the user perceives the error. The upper topoplots are related to error trials. The lower topoplots are related to correct trials.*

Figure 3.4: Grand-Average S2: *Averages of error trials (red curves), of correct trials (blue curves), and the difference error-minus-correct (black curves) for **S2** for channel FCz. The dotted lines depict the standard errors. The first vertical line represents, on average, the command onset. The vertical zero line represents the instant the user perceives the error. The upper topoplots are related to correct trials. The lower topoplots are related to error trials.*

25

3.3 Cross-correlation between signals and EOG

In the experiments, subjects were asked to fix a cross in front of them attempting to minimize eye and body movements. This precautionary measure was taken to avoid introducing artifacts into the brain signal, which could interfere with the analysis. To remove the common noise components, the CAR filter was used, followed by the application of ICA. To demonstrate the successful removal of EOG from the signals, and to ensure minimal influence from ocular movements in the EEG signals, the correlation between the signals and the EOG signal was calculated. The cross-correlation analyses were conducted in three different cases: raw signals (referred to as NoFilter) versus EOG, signals filtered with only the application of CAR (referred to as CAR) versus EOG, and signals processed through both CAR and ICA (referred to as CAR+ICA) versus EOG. Results in Figure 3.5 report the correlation values of all subjects for the three distinct filtering cases. From these, it can be seen that by applying only the CAR filter, the correlation between the signals and the EOG decreases significantly compared to the NoFilter vs. EOG case. Whereas, comparing the correlation results between CAR+ICA vs. EOG and CAR vs. EOG signals showed little variation. The median correlation values for the three groups are 0.899, 0.421, and 0.311, respectively.

Furthermore, we compute an ANOVA statistical test with Bonferroni correction to evaluate the significant differences between the three correlation distributions. The outcomes of this analysis revealed statistically significant differences among the correlation values obtained from the three filtering scenarios. The statistical test confirms substantial variability and distinction among the signal groups, as highlighted in Figure 3.5. The use of the asterisk (*) means that the two groups are statistically different with a significance level of 0.05.

Individual analysis of the cross-correlation results for each subject reveals that, among the 9 subjects, 7 exhibit comparable cross-correlation outcomes between CAR versus EOG and CAR+ICA versus EOG. As an example, Figure 3.6 shows S6 results, embracing this observation, while the results for S2 deviate from this trend. Additionally, single-subject ANOVA test results are represented with asterisks (*) in Figure 3.6, showing the groups that are statistically different with a significance level of 0.05. All the other subjects' results are reported in Appendix B.

3.4 Classification results

To evaluate the ability to detect ErrPs on a trial-by-trial basis, classification was performed by dividing all trials into training and test sets. This strategy ensured that testing was always performed on different data than the ones used to train the model, thus ensuring that the model's performance was rigorously assessed on unseen data, preventing overfitting and validating the
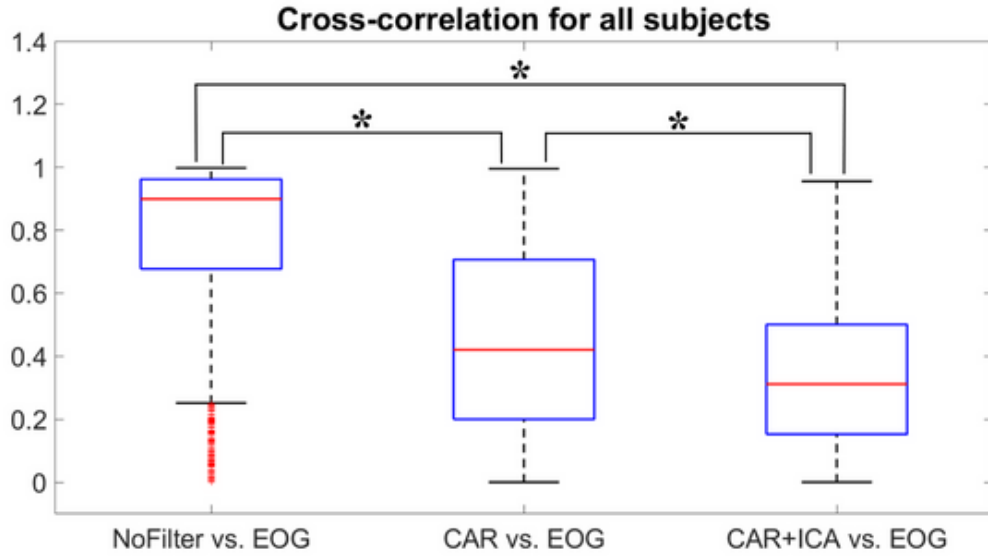
Figure 3.5: All subjects cross-correlation: *Cross-correlation results for all subjects for the three cases: NoFilter vs. EOG; CAR vs. EOG; CAR+ICA vs. EOG. The asterisks are the results of the ANOVA test (the two groups are statistically different).*
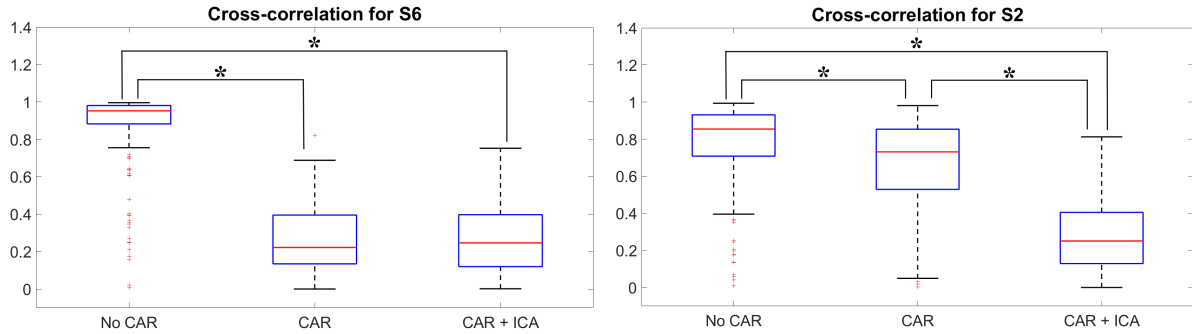

Figure 3.6: Single subjects cross-correlation: *On the left: cross-correlation results for subject S6, showing good results of CAR filter. On the right: cross-correlation results for subject S2 for which the CAR filter is not removing the EOG component. The asterisks are the results of the ANOVA test (the two groups are statistically different).*

model's generalizability. Both training and test sets classification results were analyzed utilizing the AUC values, the accuracy, the sensitivity, and the specificity. The average AUC was 0.9423 ± 0.0454 for the training set and 0.7922 ± 0.1362 for the test set; the average accuracy was 82.6889 ± 11.5406 for the training set and 79.5000 ± 10.3285 for the test set; the average sensitivity was 82.4000 ± 12.9546 for the training set and 80.3111 ± 11.4585 for the test set; the average specificity was 89.0556 ± 14.4664 for the training set and 68.1111 ± 11.8334 for the test set. The AUC results are reported in Figure 3.7, while the other metrics are depicted in Table 3.1 presenting a comprehensive depiction of the model's performance. Additionally, the feature extraction process required a careful selection of subject-specific channels critical for classifica-

tion. Table 3.2 details the channels selected for each subject, underlining the tailored approach employed in the selection, thus optimizing the classification process.
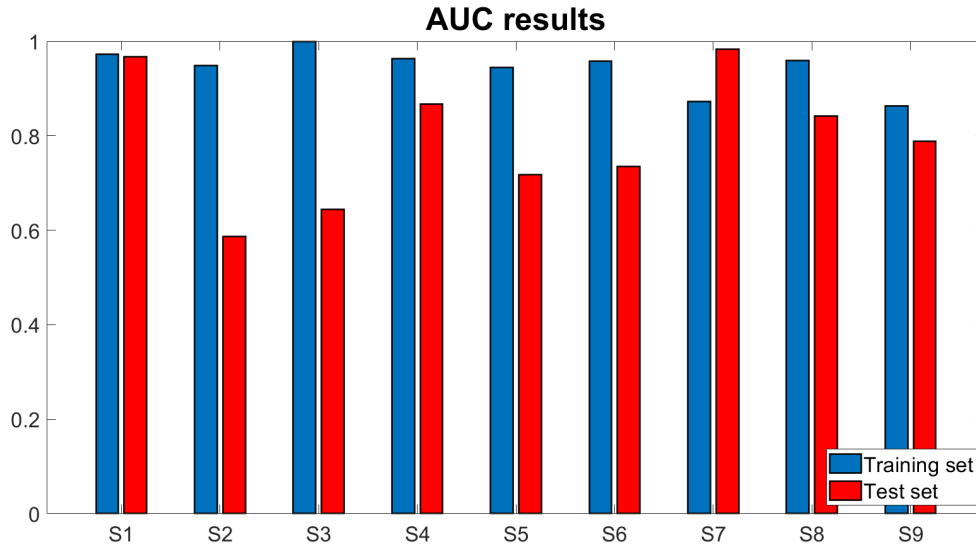

Figure 3.7: Classification results: *Classification results determined by the AUC for the training set (blue bar) and test set (red bar) for the 9 different subjects.*

Table 3.1: Classification results: *The results are all expressed in percentage (%). The table reports the accuracy, sensitivity, and specificity results for both the training set and test set for all subjects.*

Subjects	Results training set			Results test set		
	Accuracy	Sensitivity	Specificity	Accuracy	Sensitivity	Specificity
S1	95.9	99	64	87	87.5	80
S2	60	57	100	64	64	66.6
S3	97.6	97.5	100	86.5	90.9	50
S4	86.4	86.4	87.5	80.4	81.6	50
S5	73.7	72	100	73.5	73.9	66.7
S6	80	78.6	100	71	69	83
S7	84.3	85.7	70	98	100	75
S8	88.1	87.4	100	72.6	72.9	66.7
S9	78.2	78	80	82.5	83	75

Table 3.2: Selected channels: *Channels selected for the classification procedure to recognize the ErrP*

Subjects	Selected channels
S1	Fz, Cz, FCz
S2	Fz, Cz, FCz
S3	Fz, FCz
S4	Fz, Cz
S5	Fz, Cz, FCz
S6	Fz, Cz, FCz
S7	Fz, Cz
S8	Fz, Pz
S9	FCz

3.4.1 Sliding window classification

For the sliding window classification, the previously created classifier was used to evaluate the performance on the test set through the use of sliding windows. As already highlighted, in this case, the start of the trials corresponds to the command onset. The results offer a perspective on the classifier's performance across the different segments. By focusing on the AUC, the time shift that corresponds to the highest AUC value was analyzed. This shift was compared with the average delay applied to the trials. The results (Table 3.3) show that, in most cases, the optimal classification using the sliding windows occurred with a time shift similar to the average delay. This outcome highlights that the delay applied was reasonable.

For illustrative purposes, the AUC results of a single subject are reported. However, it is important to note that similar analyses were conducted across all subjects. All the results are presented in Appendix C. Figure 3.8 provides a visualization of the AUC values corresponding to the different windows for Subject 7. As shown in Figure 3.8, the highest AUC corresponds to a shift from the command onset of 25 samples which is equal to 0.3906 seconds, comparable to the mean delay applied (0.3982 seconds).

To consolidate the sliding window classification results for each trial across all windows, subject-specific thresholds are used on the predicted posterior probabilities. Based on the thresholds, each trial is classified as correct or error trial, and based on the classification results the recognition rates were computed. Table 3.4 shows the recognition rates (accuracy, sensitivity, and specificity) for all subjects. These rates reflect the efficacy of the classifier in accurately categorizing trials based on different temporal windows, providing a summary of the classifier's performance.

***Figure 3.8: AUC results**: AUC results for S7. The vertical line represents the highest AUC value corresponding to the shift equal to 25*

***Table 3.3: Comparison between the shift related to the highest AUC and the mean delay applied:** for each subject, the table highlights the mean delay applied to the trials in the processing, the shift corresponding to the highest AUC values in seconds, and the difference between the mean delay and the shift.*

Subjects	mean delay [s]	shift [s]	difference [s]
S1	0.3838	0.4375	-0.0537
S2	0.3735	0.3125	0.0610
S3	0.3430	0.4844	-0.1414
S4	0.2898	0.2500	0.0398
S5	0.3361	0.2500	0.0861
S6	0.3722	0.5000	-0.1278
S7	0.3982	0.3906	0.0076
S8	0.3641	0.2813	0.0828
S9	0.2874	0.2656	0.0218

***Table 3.4: Recognition rates:** The table reports the recognition rates: accuracy, sensitivity, and specificity for each subject in percentage (%).*

Subjects	Accuracy	Sensitivity	Specificity
S1	96	98	80
S2	90.8	94	33.3
S3	75.7	75.8	75
S4	78.4	79.6	50
S5	63.3	65.2	33.3
S6	78.2	83.4	33.3
S7	70	69.6	75
S8	77.4	78	66.7
S9	82.5	83	75

Chapter 4

Discussion

4.1 Delay analysis

Understanding when the user perceives an error is a fundamental aspect of the study of human-computer interaction. In particular, research studies focusing on the analysis of ErrP within a real device such as a wheelchair are still limited. The limited availability of such research underlines the fundamental need to consider delay as a critical parameter. Exploring these delays in users' interaction with real-world devices provides valuable insights into the complexities of error perception. This research fills a significant gap in the understanding of ErrP in the practical context of wheelchair control. By deepening the analysis of delays, it aims to elucidate the temporal complexities involved in wheelchair movement, of error perception, paving the way for a deeper understanding of human-computer interaction in the context of real-world devices. Observing and analyzing the mean values of the delays, shown in Figure 3.1, reveals differences in the perception times of each subject, highlighting variations in cognitive processing and reaction times specific to each individual. Time delays may be influenced by variables such as prior experience and cognitive strategies used when interacting with the wheelchair control system. Understanding the impact of these variables is crucial and may provide a deeper perspective on subjective error perception, given the importance of customizing analysis according to individual user characteristics.

4.2 Grand-Average analysis

The main aim of this research was to investigate ErrP during the active control of a powered wheelchair. We tried to understand the brain response by analyzing the EEG signals during instances when the users perceived or did not perceive errors from the system over which they have no control. The experimental data collected from nine subjects allowed a comparative

visualization and analysis of the brain responses during error and correct trials in the selected channels. The results presented in Figure 3.2 provide an insight into the average neural activity observed in response to error and correct actions of the wheelchair and offer an overview of the appearance and characteristics of ErrP in the brain regions examined. In Figure 3.2, it is possible to notice a different brain response for the two classes. In particular, a positive peak at 0.17 seconds, followed by a negative peak at 0.373 seconds, and a second positive peak at 0.64 seconds distinguish the error trials. Additionally, the topoplots highlight the difference between the correct and error trials.

The single-subject brain response results confirm the existence of ErrP and show a different brain response between error and correct actions. They also show significant differences in the ErrPs recorded between the different subjects, both in the shape and in the timing of the peaks. For some subjects like S4, a clear and well-defined ErrP curve is observed, whereas for others like S2, a less distinct and more difficult to identify ErrP is detected. This variability in response underlines a difference between subjects in the reaction to an erroneous action, making it more complex to discriminate between error and correct trials. The main discriminator for all subjects in identifying the ErrP seems to be the negative deflection, which is present in error trials but not in the correct ones. The average latency of the negative peak from the user perception of the error is 0.2944 ± 0.1119 seconds. The positive peaks, on the other hand, often appear in both correct and error trials, which could be related to the P300 component. The average latency of the positive peak from the user perception of the command is 0.1050 ± 0.0943. It is possible that, after a certain number of trials, users become used to the presence of the error and no longer react with surprise to the incorrect action. At the same time, the execution of the correct command could produce a surprise effect in the user, contributing to the appearance of the P300. Moreover, upon examining the grand average of S2, it becomes evident that the mean error trials and mean correct trials exhibit a significant similarity. Both response patterns show a nearly identical trend. This convergence might be attributed to the subject's familiarity with the experiment and the control protocol. Given the subject's awareness of ErrPs, it resulted in a similar surprise reaction observed in both correct and error trials. The subject was not able to focus exclusively on the control of the wheelchair and the accurate movement execution but continued to anticipate the occurrence of the errors. The user's driving behavior was strongly influenced by this awareness, taking preventive actions to be able to correct any errors and return to the desired position. Furthermore, being aware of the presence of errors, he showed surprise when the wheelchair correctly executed the command, generating a P300. At the same time, if the command was executed incorrectly, the ErrP was generated, although with a reduced amplitude. This phenomenon is in line with the findings in the literature [42], where it is observed that the amplitude of the ErrP decreases as the frequency of errors increases and, consequently,

the subject's adaptation to the continuous presence of errors in the experiment.

4.3   Influence of EOG in the detection of ErrP

Artifacts in the EEG can be caused by physiological activity such as eye movements, blinking, electrocardiographic activity, and muscle movements. Bandpass filters are usually used to remove such artifacts because the frequencies associated with these physiological signals are well-known. In addition, the CAR filter is often used to reduce or remove the common components to all EEG channels. However, there are other methods of artifact removal, including ICA, which further clean up the signal. It is important to note that ICA is not suitable for real-time analysis and therefore is not applicable online. To ensure consistency between offline and online analysis, it is desirable to avoid using ICA during offline analysis. As described previously, the similarity of the noFilter, CAR, CAR+ICA signals to the EOG was assessed. The results indicate that the application of the CAR filter removes much of the common noise present in all channels of the EEG, including eye movements, in almost all subjects. Subsequent integration of the ICA did not appear to result in significant improvements for most subjects, with the exception of two cases. This could be due to the fact that the initial correlation between CAR and EOG was already low. However, for the remaining two subjects a significant improvement is observed: the correlation between CAR+ICA and EOG signals decreases significantly. This could indicate that ICA has removed many components including movement-related artifacts. In fact, we know that these two subjects did not restrict their body movements, suggesting a greater effect of ICA signal cleaning. As a consequence of these results, even if the groups are statistically different, it was decided to carry out the subsequent analysis using the data filtered only by the CAR filter because the correlation values were still low. This decision was made to facilitate future online implementation, as ICA cannot be implemented online. These findings collectively emphasize the efficacy of the CAR filter in attenuating EOG-related artifacts from EEG signals.

4.4   Decoding ErrP

The classification results demonstrate the possibility to discriminate between error and correct trials during the navigation with a powered wheelchair. These outcomes exhibit a generally satisfactory performance observed for most participants, stating the efficacy of the classification model. However, for S3 and S4, it can be noticed that the classification performance is mainly high for the positive class (correct trials). This situation leads to good overall accuracy, but a detailed examination of the specificity shows that the results reflect performance metrics similar

to those of a random classifier. In general, the classifier is able to effectively identify true negatives and true positives while minimizing false positives and false negatives. It is essential to underline that leave-one-out cross-validation (LOOCV) was not adopted to create the classifier. This decision was made in view of our final objective, which is the future implementation of the protocol online. LOOCV, although a common practice for evaluating classifiers, is not compatible with our ultimate goal of implementing the protocol in real-time. Since LOOCV involves the sequential exclusion of a single sample for validation, in the context of an online application, the implementation of LOOCV could introduce difficulties in adapting the classifier to the real-time data stream, limiting its effectiveness and usability in practical use. Therefore, although LOOCV is a valid practice for classifier evaluation, its application in this specific context was not considered suitable for our research objectives.

4.4.1   Sliding window classification discussion

The implementation of sliding window classification was used to simulate real-time classification, providing an analysis of the classifier's capability to detect ErrPs within segmented temporal windows following the command onset. This analysis was carried out to avoid the complexity associated with computing the delay. In the context of a real-time application, determining the delay between the command and the user's perception of the command execution can be challenging and impractical. Therefore, we adopted the sliding window approach that enables us to directly focus on the command-onset event as the starting point for ErrP classification. Moreover, the implementation of subject-specific thresholds based on predicted posterior probabilities adds a crucial layer of individualization, considering variations in temporal dynamics and individual response patterns. As the results show, the observed shift time associated with the highest AUC value aligns with the applied delay for most of the subjects. This suggests that the selected window for trial extraction is pertinent to the analysis. The classification with the sliding window reports lower recognition rates compared to the previous classification.

Chapter 5

Conclusions

The research focused on analyzing the brain response during discrete control of a powered wheelchair. The results showed a significant difference in the responses between correct and wrong actions, confirming the possibility to identify ErrPs following incorrect commands. Furthermore, we developed a classifier capable of successfully decoding erroneous responses on a trial-by-trial basis, with consistent and promising classification results for future online implementation. However, it turned out that neural activity varies considerably from subject to subject, making it complex to create a universal interface suitable for all users. Therefore, individual training steps to optimize system parameters are essential.

Despite the successful findings, there is still much to be explored and several aspects require further investigation. These include improving signal decoding in more complex environments without a predefined path to better simulate realistic scenarios. It is also essential to test the system on people with disabilities and characterize their neural response, as they will be the final users of the device. It is also essential to evaluate the system online to verify its effectiveness in recognizing and correcting errors and to integrate it with the MI BCI system to improve overall performances.

It should be emphasized that, although discrete control represents an important step, it is based on separate and distinct commands. It is similar to moving in steps, with each command representing a single movement. Therefore, this type of control may not appear natural to the user. On the other hand, continuous control is more like a smooth and uninterrupted movement. Continuous control might be perceived as more intuitive and closer to the natural experience of driving than discrete control. Therefore, continuous control may be more appropriate in everyday contexts. This suggests the need to develop solutions that integrate continuous control to ensure a smoother experience adaptable to real-world use.

Another important aspect to consider is eye movement, which adds complexity to the analysis. During the experiment, users were required to focus on a cross, but this condition may be un-

realistic and uncomfortable in a real-world implementation. It is therefore important to assess how eye movements affect the signals when the user is free to move their eyes and how these artifacts may affect the analysis.

In conclusion, this study is an important step forward in research and provides a basis for future studies and developments with the final aim of helping people with motor impairments in everyday life.

Bibliography

[1] L. F. Nicolas-Alonso and J. Gomez-Gil, «Brain computer interfaces, a review», *sensors*, vol. 12, no. 2, pp. 1211–1279, 2012.

[2] J. J. Shih, D. J. Krusienski, and J. R. Wolpaw, «Brain-computer interfaces in medicine», in *Mayo clinic proceedings*, Elsevier, vol. 87, 2012, pp. 268–279.

[3] I. Lazarou, S. Nikolopoulos, P. C. Petrantonakis, I. Kompatsiaris, and M. Tsolaki, «Eeg-based brain–computer interfaces for communication and rehabilitation of people with motor impairment: A novel approach of the 21 st century», *Frontiers in human neuroscience*, vol. 12, p. 14, 2018.

[4] Z. Gao, Z. Pang, Y. Chen, *et al.*, «Restoring after central nervous system injuries: Neural mechanisms and translational applications of motor recovery», *Neuroscience Bulletin*, vol. 38, no. 12, pp. 1569–1587, 2022.

[5] H. Lorach, A. Galvez, V. Spagnolo, *et al.*, «Walking naturally after spinal cord injury using a brain–spine interface», *Nature*, pp. 1–8, 2023.

[6] A. N. Belkacem, N. Jamil, S. Khalid, and F. Alnajjar, «On closed-loop brain stimulation systems for improving the quality of life of patients with neurological disorders», *Frontiers in Human Neuroscience*, vol. 17, p. 1 085 173, 2023.

[7] J. Mang, Z. Xu, Y. Qi, and T. Zhang, «Favoring the cognitive-motor process in the closed-loop of bci mediated post stroke motor function recovery: Challenges and approaches», *Frontiers in Neurorobotics*, vol. 17, 2023.

[8] S. Perdikis, L. Tonin, S. Saeedi, C. Schneider, and J. d. R. Millán, «The cybathlon bci race: Successful longitudinal mutual learning with two tetraplegic users», *PLoS biology*, vol. 16, no. 5, e2003787, 2018.

[9] U. Salahuddin and P.-X. Gao, «Signal generation, acquisition, and processing in brain machine interfaces: A unified review», *Frontiers in Neuroscience*, p. 1174, 2021.

[10] S. Waldert, «Invasive vs. non-invasive neuronal signals for brain-machine interfaces: Will one prevail?», *Frontiers in neuroscience*, vol. 10, p. 295, 2016.

[11] Z.-P. Zhao, C. Nie, C.-T. Jiang, *et al.*, «Modulating brain activity with invasive brain–computer interface: A narrative review», *Brain Sciences*, vol. 13, no. 1, p. 134, 2023.

[12] M Tudor, L Tudor, and K. Tudor, «Hans berger (1873-1941)-povijest elektroencefalografije», *ACTA MEDICA CROATICA*, vol. 59, no. 4, p. 307, 2005.

[13] S. Saha, K. A. Mamun, K. Ahmed, *et al.*, «Progress in brain computer interface: Challenges and opportunities», *Frontiers in Systems Neuroscience*, vol. 15, p. 578 875, 2021.

[14] A. Y. Chan, B. V. Lien, N. J. Brown, *et al.*, «Utility of adding electrodes in patients undergoing invasive seizure localization: A case series», *Annals of Medicine and Surgery*, vol. 80, p. 104 139, 2022.

[15] N. K. Logothetis, «What we can do and what we cannot do with fmri», *Nature*, vol. 453, no. 7197, pp. 869–878, 2008.

[16] G. H. Glover, «Overview of functional magnetic resonance imaging», *Neurosurgery Clinics*, vol. 22, no. 2, pp. 133–139, 2011.

[17] V. Scarapicchia, C. Brown, C. Mayo, and J. R. Gawryluk, «Functional magnetic resonance imaging and functional near-infrared spectroscopy: Insights from combined recording studies», *Frontiers in human neuroscience*, vol. 11, p. 419, 2017.

[18] R. Li, D. Yang, F. Fang, K.-S. Hong, A. L. Reiss, and Y. Zhang, «Concurrent fnirs and eeg for brain function investigation: A systematic, methodology-focused review», *Sensors*, vol. 22, no. 15, p. 5865, 2022.

[19] S. P. Singh, «Magnetoencephalography: Basic principles», *Annals of Indian Academy of Neurology*, vol. 17, no. Suppl 1, S107, 2014.

[20] R. Hari and R. Salmelin, «Magnetoencephalography: From squids to neuroscience: Neuroimage 20th anniversary special edition», *Neuroimage*, vol. 61, no. 2, pp. 386–396, 2012.

[21] M. Orban, M. Elsamanty, K. Guo, S. Zhang, and H. Yang, «A review of brain activity and eeg-based brain–computer interfaces for rehabilitation application», *Bioengineering*, vol. 9, no. 12, p. 768, 2022.

[22] M. K. Islam and A. Rastegarnia, «Recent advances in eeg (non-invasive) based bci applications», *Frontiers in Computational Neuroscience*, vol. 17, p. 1 151 852, 2023.

[23] P. Campisi and D. La Rocca, «Brain waves for automatic biometric-based user recognition», *IEEE transactions on information forensics and security*, vol. 9, no. 5, pp. 782–800, 2014.

[24] R. Portillo-Lara, B. Tahirbegi, C. A. Chapman, J. A. Goding, and R. A. Green, «Mind the gap: State-of-the-art technologies and applications for eeg-based brain–computer interfaces», *APL bioengineering*, vol. 5, no. 3, 2021.

[25]   S. Kwon, J. Kim, and T. Kim, «Neuropsychological activations and networks while performing visual and kinesthetic motor imagery», *Brain Sciences*, vol. 13, no. 7, 2023, issn: 2076-3425. doi: 10.3390/brainsci13070983. [Online]. Available: https://www.mdpi.com/2076-3425/13/7/983.

[26]   E. Naito, T. Morita, and K. Amemiya, «Body representations in the human brain revealed by kinesthetic illusions and their essential contributions to motor control and corporeal awareness», *Neuroscience Research*, vol. 104, pp. 16–30, 2016.

[27]   K. J. Miller, G. Schalk, E. E. Fetz, M. Den Nijs, J. G. Ojemann, and R. P. Rao, «Cortical activity during motor execution, motor imagery, and imagery-based online feedback», *Proceedings of the National Academy of Sciences*, vol. 107, no. 9, pp. 4430–4435, 2010.

[28]   T. Mulder, «Motor imagery and action observation: Cognitive tools for rehabilitation», *Journal of neural transmission*, vol. 114, pp. 1265–1278, 2007.

[29]   R. Srinivasan, W. R. Winter, and P. L. Nunez, «Source analysis of eeg oscillations using high-resolution eeg and meg», *Progress in brain research*, vol. 159, pp. 29–42, 2006.

[30]   O.-Y. Kwon, M.-H. Lee, C. Guan, and S.-W. Lee, «Subject-independent brain–computer interfaces based on deep convolutional neural networks», *IEEE transactions on neural networks and learning systems*, vol. 31, no. 10, pp. 3839–3852, 2019.

[31]   R. Rupp, «Challenges in clinical applications of brain computer interfaces in individuals with spinal cord injury», *Frontiers in neuroengineering*, vol. 7, p. 38, 2014.

[32]   T. Warbrick, «Simultaneous eeg-fmri: What have we learned and what does the future hold?», *Sensors*, vol. 22, no. 6, p. 2262, 2022.

[33]   J. Gutierrez-Martinez, J. A. Mercado-Gutierrez, B. E. Carvajal-Gámez, J. L. Rosas-Trigueros, and A. E. Contreras-Martinez, «Artificial intelligence algorithms in visual evoked potential-based brain-computer interfaces for motor rehabilitation applications: Systematic review and future directions», *Frontiers in Human Neuroscience*, vol. 15, p. 772 837, 2021.

[34]   A. M. Husain, *Illustrated manual of clinical evoked potentials*. Springer Publishing Company, 2017.

[35]   M. Nakanishi, Y. Wang, Y.-T. Wang, Y. Mitsukura, and T.-P. Jung, «Generating visual flickers for eliciting robust steady-state visual evoked potentials at flexible frequencies using monitor refresh rate», *PloS one*, vol. 9, no. 6, e99235, 2014.

[36]   F.-B. Vialatte, M. Maurice, J. Dauwels, and A. Cichocki, «Steady-state visually evoked potentials: Focus on essential paradigms and future perspectives», *Progress in neurobiology*, vol. 90, no. 4, pp. 418–438, 2010.

[37] R. Mertens and J. Polich, «P300 from a single-stimulus paradigm: Passive versus active tasks and stimulus modality», *Electroencephalography and Clinical Neurophysiology/Evoked Potentials Section*, vol. 104, no. 6, pp. 488–497, 1997.

[38] S. Debener, S. Makeig, A. Delorme, and A. K. Engel, «What is novel in the novelty oddball paradigm? functional significance of the novelty p3 event-related potential as revealed by independent component analysis», *Cognitive Brain Research*, vol. 22, no. 3, pp. 309–321, 2005.

[39] E. Donchin, K. Spencer, and R. Wijesinghe, «The mental prosthesis: Assessing the speed of a p300-based brain-computer interface», *IEEE Transactions on Rehabilitation Engineering*, vol. 8, no. 2, pp. 174–179, 2000. doi: 10.1109/86.847808.

[40] T. W. Picton *et al.*, «The p300 wave of the human event-related potential», *Journal of clinical neurophysiology*, vol. 9, pp. 456–456, 1992.

[41] F. Li, C. Yi, Y. Jiang, *et al.*, «Different contexts in the oddball paradigm induce distinct brain networks in generating the p300», *Frontiers in human neuroscience*, vol. 12, p. 520, 2019.

[42] P. W. Ferrez and J. del R. Millán, «Error-related eeg potentials generated during simulated brain–computer interaction», *IEEE Transactions on Biomedical Engineering*, vol. 55, pp. 923–929, 2008. [Online]. Available: https://api.semanticscholar.org/CorpusID:1189113.

[43] A. Kumar, L. Gao, E. Pirogova, and Q. Fang, «A review of error-related potential-based brain–computer interfaces for motor impaired people», *IEEE Access*, vol. 7, pp. 142451–142466, 2019.

[44] A. Etkin, T. Egner, and R. Kalisch, «Emotional processing in anterior cingulate and medial prefrontal cortex», *Trends in cognitive sciences*, vol. 15, no. 2, pp. 85–93, 2011.

[45] J. Omedes, A. Schwarz, G. R. Müller-Putz, and L. Montesano, «Factors that affect error potentials during a grasping task: Toward a hybrid natural movement decoding bci», *Journal of neural engineering*, vol. 15, no. 4, p. 046023, 2018.

[46] A. Xavier Fidêncio, C. Klaes, and I. Iossifidis, «Error-related potentials in reinforcement learning-based brain-machine interfaces», *Frontiers in Human Neuroscience*, vol. 16, p. 806517, 2022.

[47] M. Mousavi and V. R. de Sa, «Spatio-temporal analysis of error-related brain activity in active and passive brain–computer interfaces», *Brain-computer interfaces*, vol. 6, no. 4, pp. 118–127, 2019.

[48] R. Chavarriaga and J. d. R. Millán, «Learning from eeg error-related potentials in noninvasive brain-computer interfaces», *IEEE transactions on neural systems and rehabilitation engineering*, vol. 18, no. 4, pp. 381–388, 2010.

[49] P. W. Ferrez and J. d. R. Millán, «Simultaneous real-time detection of motor imagery and error-related potentials for improved bci accuracy», in *Proceedings of the 4th international brain-computer interface workshop and training course*, 2008, pp. 197–202.

[50] A. Palumbo, V. Gramigna, B. Calabrese, and N. Ielpo, «Motor-imagery eeg-based bcis in wheelchair movement and control: A systematic literature review», *Sensors*, vol. 21, no. 18, p. 6285, 2021.

[51] C. S. L. Tsui, J. Q. Gan, and H. Hu, «A self-paced motor imagery based brain-computer interface for robotic wheelchair control», *Clinical EEG and neuroscience*, vol. 42, no. 4, pp. 225–229, 2011.

[52] J. Li, J. Liang, Q. Zhao, J. Li, K. Hong, and L. Zhang, «Design of assistive wheelchair system directly steered by human thoughts», *International journal of neural systems*, vol. 23, no. 03, p. 1 350 013, 2013.

[53] L. Tonin, S. Perdikis, T. D. Kuzu, *et al.*, «Learning to control a bmi-driven wheelchair for people with severe tetraplegia», *Iscience*, vol. 25, no. 12, 2022.

[54] C. Messiou, D. Fusaro, G. Beraldo, and L. Tonin, «Real-time free space semantic segmentation for detection of traversable space for an intelligent wheelchair», in *2022 International Conference on Rehabilitation Robotics (ICORR)*, 2022, pp. 1–6. doi: `10.1109/ICORR55369.2022.9896524`.

[55] W Cobb, G. B. London, H Gastaut, *et al.*, «Report of the committee on methods of clinical examination in electroencephalography», *Electroencephalography and clinical neurophysiology*, vol. 10, no. 2, pp. 370–375, 1958.

[56] M. Seeck, L. Koessler, T. Bast, *et al.*, «The standardized eeg electrode array of the ifcn», *Clinical Neurophysiology*, vol. 128, no. 10, pp. 2070–2077, 2017, issn: 1388-2457. doi: `https://doi.org/10.1016/j.clinph.2017.06.254`. [Online]. Available: `https://www.sciencedirect.com/science/article/pii/S1388245717304832`.

[57] A. Neuro. «Clinical cap catalogue». (), [Online]. Available: `https://www.ant-neuro.com/sites/default/files/SLS-SM-0243.01rev01_WG_Clinical_Cap_Catalogue.pdf`.

[58] S. J. Luck, *An introduction to the event-related potential technique*. MIT press, 2014.

[59] P. L. Nunez and R. Srinivasan, *Electric fields of the brain: the neurophysics of EEG*. Oxford University Press, USA, 2006.

[60] ROS.org. «Ros/introduction». (), [Online]. Available: `https://wiki.ros.org/ROS/Introduction`.

[61] L. Tonin, G. Beraldo, S. Tortora, and E. Menegatti, «Ros-neuro: An open-source platform for neurorobotics», *Frontiers in Neurorobotics*, vol. 16, 2022, issn: 1662-5218. doi: `10.3389/fnbot.2022.886050`. [Online]. Available: `https://www.frontiersin.org/articles/10.3389/fnbot.2022.886050`.

[62] M. Quigley, K. Conley, B. Gerkey, *et al.*, «Ros: An open-source robot operating system», in *ICRA workshop on open source software*, Kobe, Japan, vol. 3, 2009, p. 5.

[63] (), [Online]. Available: `http://wiki.ros.org/roslaunch`.

[64] B. Burle, L. Spieser, C. Roger, L. Casini, T. Hasbroucq, and F. Vidal, «Spatial and temporal resolutions of eeg: Is it really black and white? a scalp current density view», *International Journal of Psychophysiology*, vol. 97, no. 3, pp. 210–220, 2015.

[65] D. Fattahi, B. Nasihatkon, and R. Boostani, «A general framework to estimate spatial and spatio-spectral filters for eeg signal classification», *Neurocomputing*, vol. 119, pp. 165–174, 2013.

[66] K. A. Ludwig, R. M. Miriani, N. B. Langhals, M. D. Joseph, D. J. Anderson, and D. R. Kipke, «Using a common average reference to improve cortical neuron recordings from microelectrode arrays», *Journal of neurophysiology*, vol. 101, no. 3, pp. 1679–1689, 2009.

[67] M. J. Alhaddad, «Common average reference (car) improves p300 speller», 2012. [Online]. Available: `https://api.semanticscholar.org/CorpusID:61614537`.

[68] T.-P. JUNG, S. MAKEIG, C. HUMPHRIES, *et al.*, «Removing electroencephalographic artifacts by blind source separation», *Psychophysiology*, vol. 37, no. 2, pp. 163–178, 2000. doi: `10.1111/1469-8986.3720163`.

[69] T.-P. Jung, S. Makeig, M. Westerfield, J. Townsend, E. Courchesne, and T. J. Sejnowski, «Removal of eye activity artifacts from visual event-related potentials in normal and clinical subjects», *Clinical Neurophysiology*, vol. 111, no. 10, pp. 1745–1758, 2000, issn: 1388-2457. doi: `https://doi.org/10.1016/S1388-2457(00)00386-2`. [Online]. Available: `https://www.sciencedirect.com/science/article/pii/S1388245700003862`.

[70] J. d. R. Millan, «You are wrong!—automatic detection of interaction errors from brain waves», Jan. 2005, pp. 1413–1418.

[71] P. W. Ferrez and J. del R. Millán, «Eeg-based brain-computer interaction: Improved accuracy by automatic single-trial error detection», in *Neural Information Processing Systems*, 2007. [Online]. Available: `https://api.semanticscholar.org/CorpusID:12829284`.

[72] X. Perrin, R. Chavarriaga, F. Colas, R. Siegwart, and J. del R. Millán, «Brain-coupled interaction for semi-autonomous navigation of an assistive robot», *Robotics and Autonomous Systems*, vol. 58, no. 12, pp. 1246–1255, 2010, Intelligent Robotics and Neuroscience, issn: 0921-8890. doi: `https://doi.org/10.1016/j.robot.2010.05.010`. [Online]. Available: `https://www.sciencedirect.com/science/article/pii/S0921889010001144`.

[73] W. W. Daniel and C. L. Cross, *Biostatistics: a foundation for analysis in the health sciences*. Wiley, 2018.

[74] T. Zeyl, E. Yin, M. Keightley, and T. Chau, «Adding real-time bayesian ranks to error-related potential scores improves error detection and auto-correction in a p300 speller», *IEEE transactions on neural systems and rehabilitation engineering*, vol. 24, no. 1, pp. 46–56, 2015.

[75] S. H. Park, J. M. Goo, and C.-H. Jo, «Receiver operating characteristic (roc) curve: Practical review for radiologists», *Korean journal of radiology*, vol. 5, no. 1, pp. 11–18, 2004.

[76] J. Fan, S. Upadhye, and A. Worster, «Understanding receiver operating characteristic (roc) curves», *Canadian Journal of Emergency Medicine*, vol. 8, no. 1, pp. 19–20, 2006. doi: `10.1017/S1481803500013336`.

Appendix A

Single-subjects grand-average
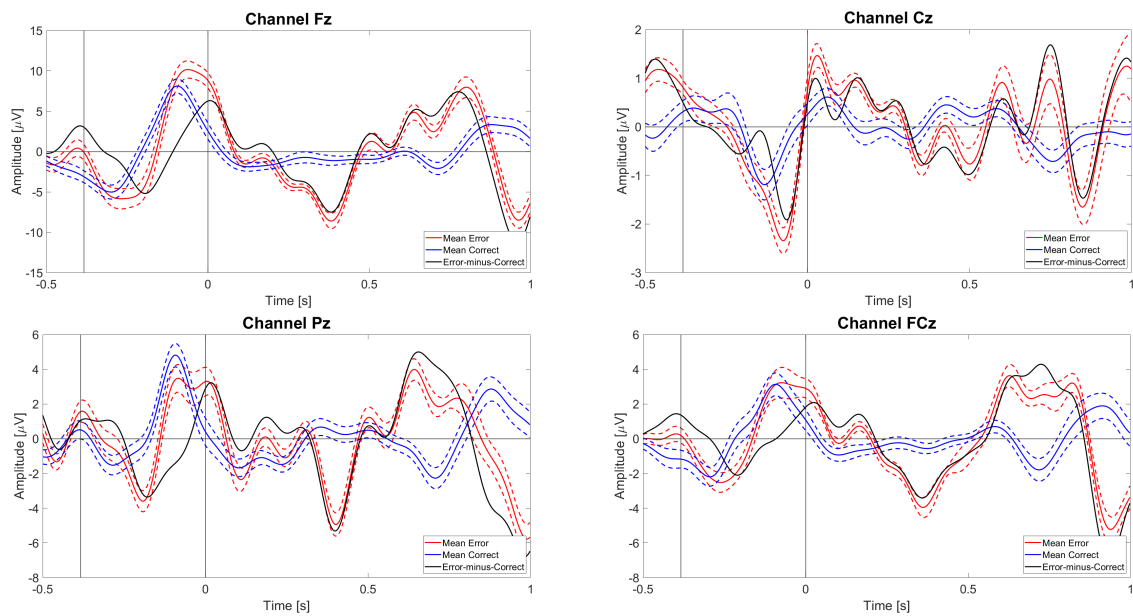
Figure A.1: Grand-Average: *Averages of error trials (red curves), of correct trials (blue curves), and the difference error-minus-correct (black curves) for **S1** for channels Fz (left-top), Cz (right-top), Pz (left-bottom), and FCz (right-bottom). The dotted lines depict the standard errors. The first vertical line represents, on average, the command onset. The vertical zero line represents the instant the user perceives the error.*
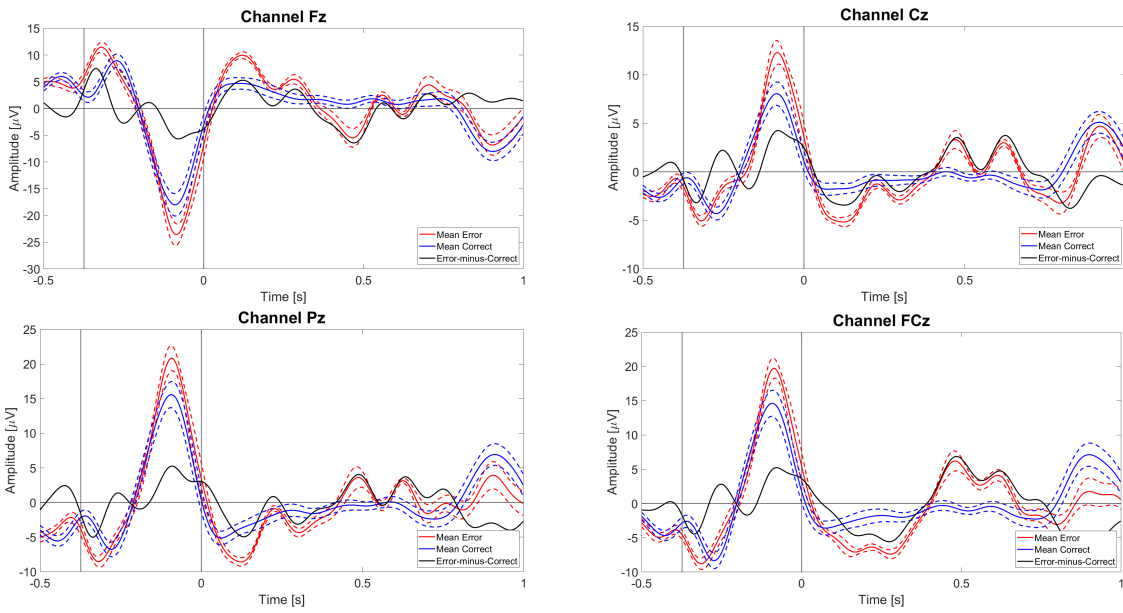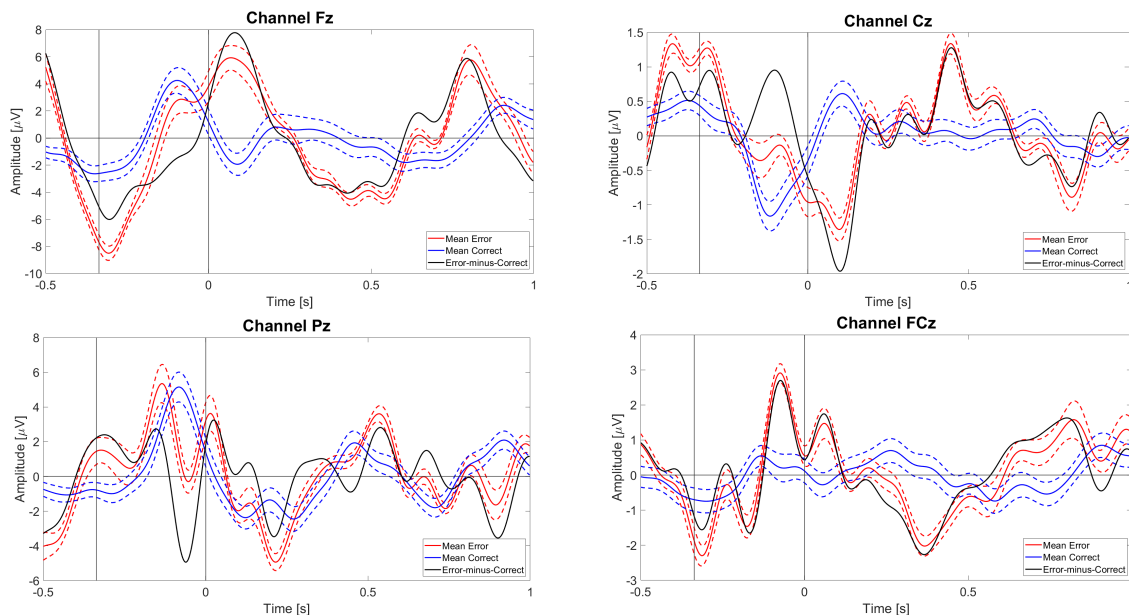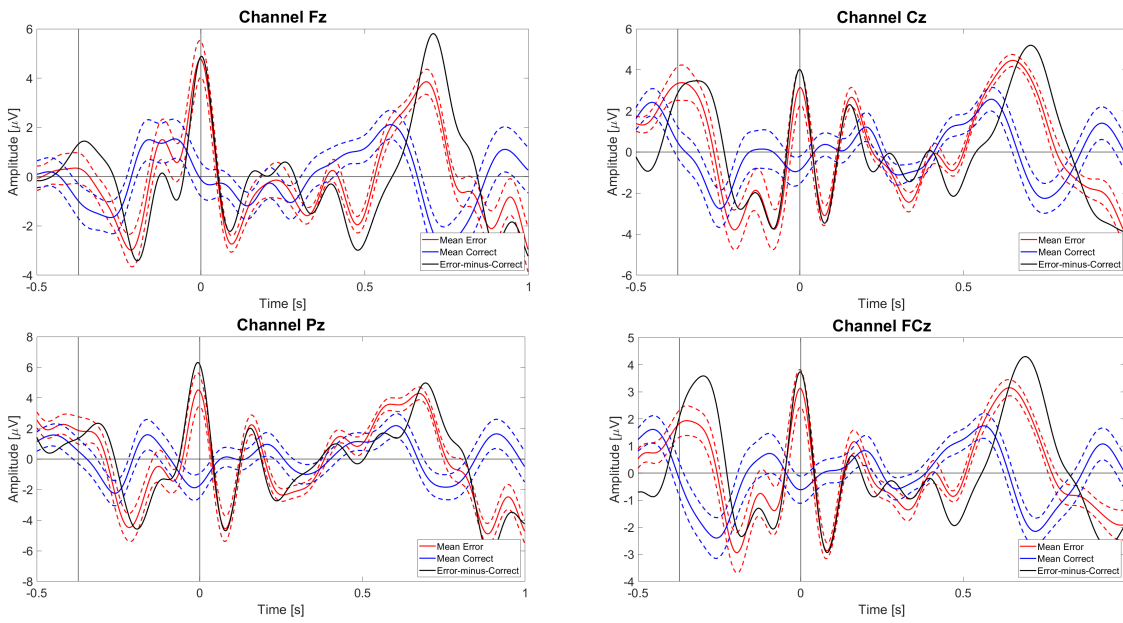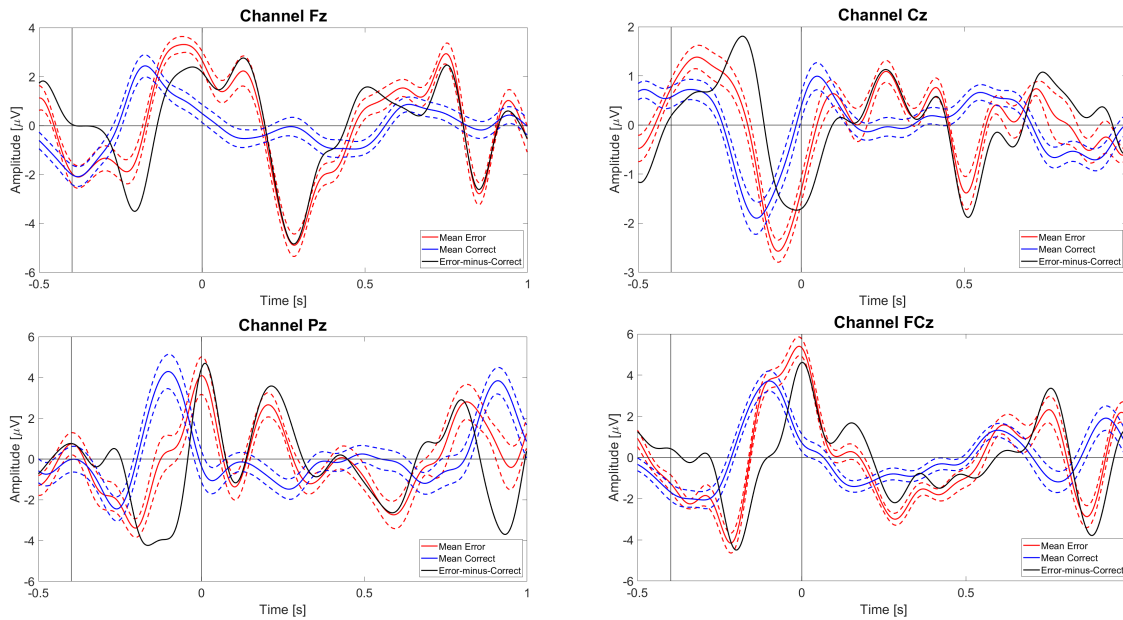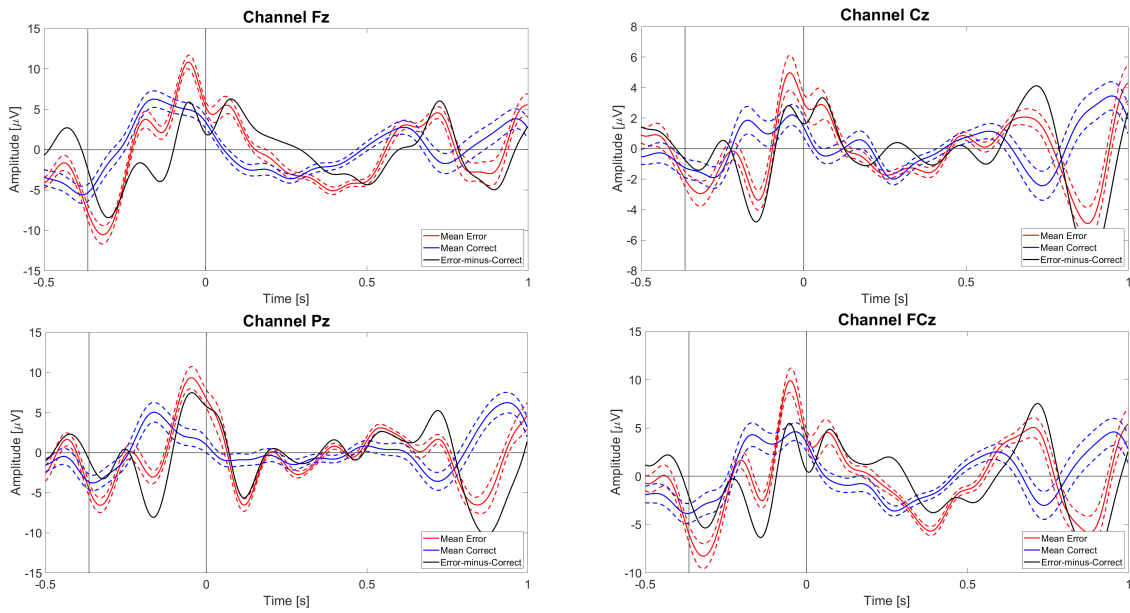
Figure A.2: Grand-Average: *Averages of error trials (red curves), of correct trials (blue curves), and the difference error-minus-correct (black curves) for **S2** for channels Fz (left-top), Cz (right-top), Pz (left-bottom), and FCz (right-bottom). The dotted lines depict the standard errors. The first vertical line represents, on average, the command onset. The vertical zero line represents the instant the user perceives the error.*
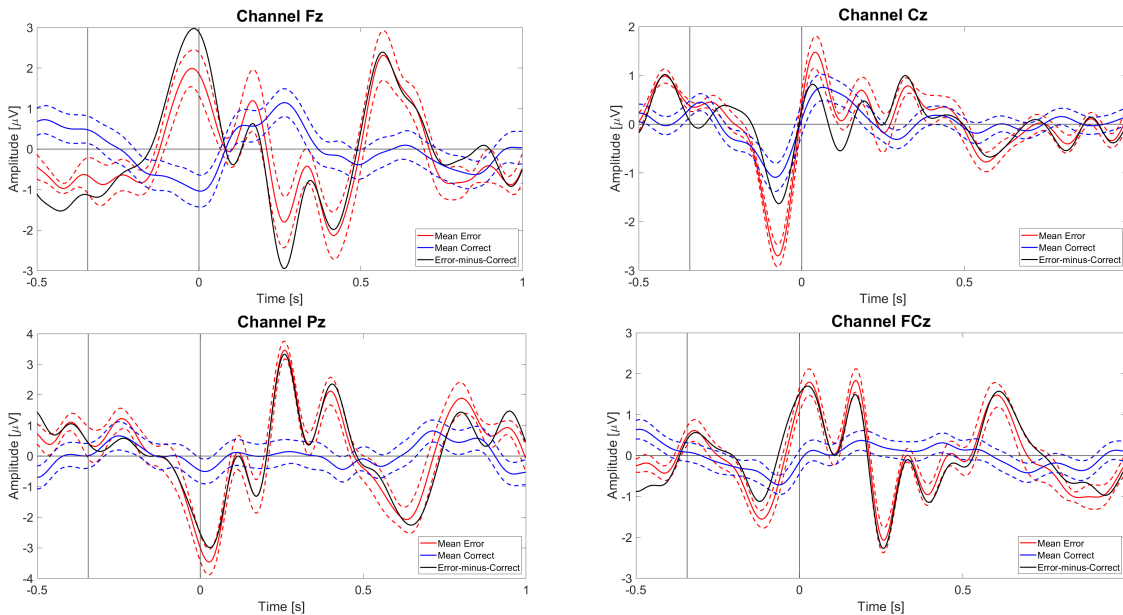
Figure A.3: Grand-Average: *Averages of error trials (red curves), of correct trials (blue curves), and the difference error-minus-correct (black curves) for **S3** for channels Fz (left-top), Cz (right-top), Pz (left-bottom), and FCz (right-bottom). The dotted lines depict the standard errors. The first vertical line represents, on average, the command onset. The vertical zero line represents the instant the user perceives the error.*
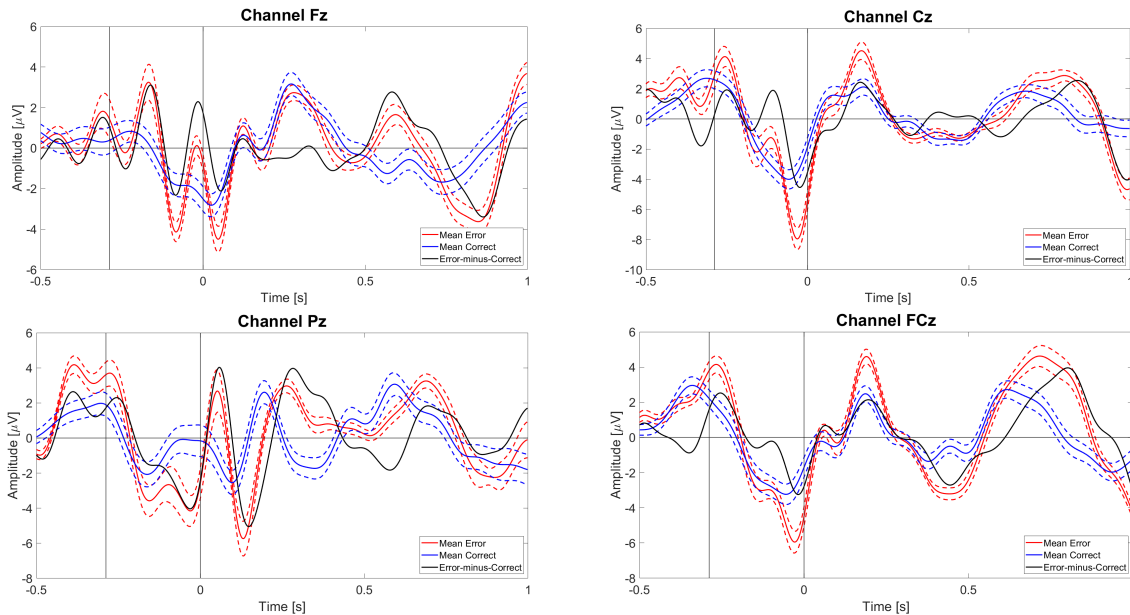
46
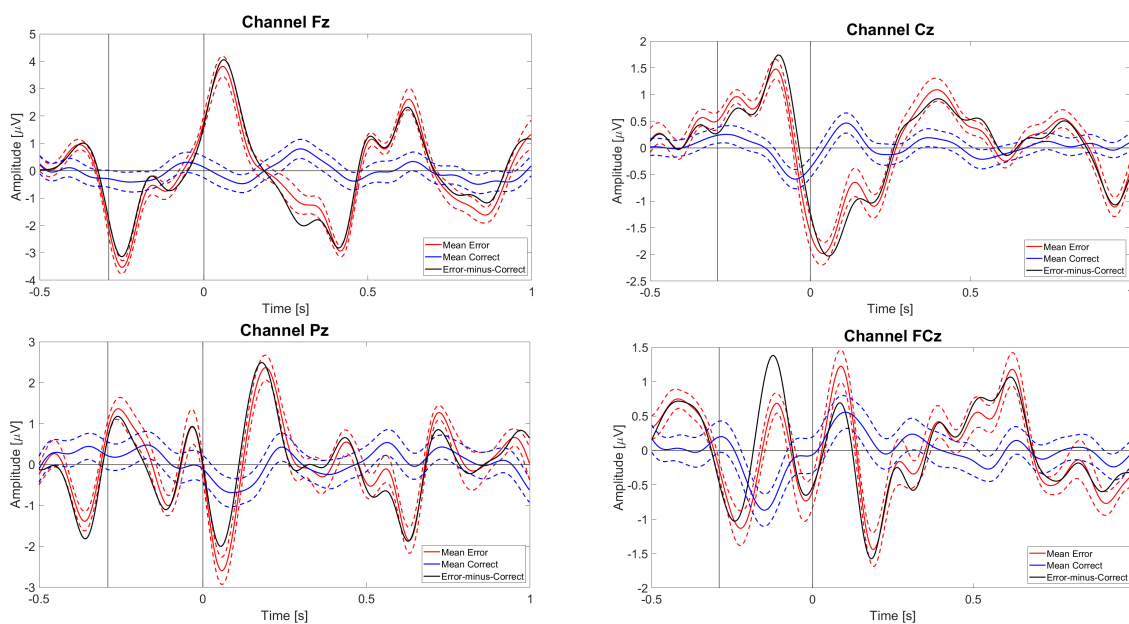
Figure A.4: Grand-Average: *Averages of error trials (red curves), of correct trials (blue curves), and the difference error-minus-correct (black curves) for **S4** for channels Fz (left-top), Cz (right-top), Pz (left-bottom), and FCz (right-bottom). The dotted lines depict the standard errors. The first vertical line represents, on average, the command onset. The vertical zero line represents the instant the user perceives the error.*

***Figure A.5: Grand-Average:*** *Averages of error trials (red curves), of correct trials (blue curves), and the difference error-minus-correct (black curves) for **S5** for channels Fz (left-top), Cz (right-top), Pz (left-bottom), and FCz (right-bottom). The dotted lines depict the standard errors. The first vertical line represents, on average, the command onset. The vertical zero line represents the instant the user perceives the error.*

47

Figure A.6: Grand-Average: *Averages of error trials (red curves), of correct trials (blue curves), and the difference error-minus-correct (black curves) for **S6** for channels Fz (left-top), Cz (right-top), Pz (left-bottom), and FCz (right-bottom). The dotted lines depict the standard errors. The first vertical line represents, on average, the command onset. The vertical zero line represents the instant the user perceives the error.*

Figure A.7: Grand-Average: *Averages of error trials (red curves), of correct trials (blue curves), and the difference error-minus-correct (black curves) for **S7** for channels Fz (left-top), Cz (right-top), Pz (left-bottom), and FCz (right-bottom). The dotted lines depict the standard errors. The first vertical line represents, on average, the command onset. The vertical zero line represents the instant the user perceives the error.*

Figure A.8: Grand-Average: *Averages of error trials (red curves), of correct trials (blue curves), and the difference error-minus-correct (black curves) for **S8** for channels Fz (left-top), Cz (right-top), Pz (left-bottom), and FCz (right-bottom). The dotted lines depict the standard errors. The first vertical line represents, on average, the command onset. The vertical zero line represents the instant the user perceives the error.*

Figure A.9: Grand-Average: *Averages of error trials (red curves), of correct trials (blue curves), and the difference error-minus-correct (black curves) for **S9** for channels Fz (left-top), Cz (right-top), Pz (left-bottom), and FCz (right-bottom). The dotted lines depict the standard errors. The first vertical line represents, on average, the command onset. The vertical zero line represents the instant the user perceives the error.*

49

Appendix B

Cross-correlation
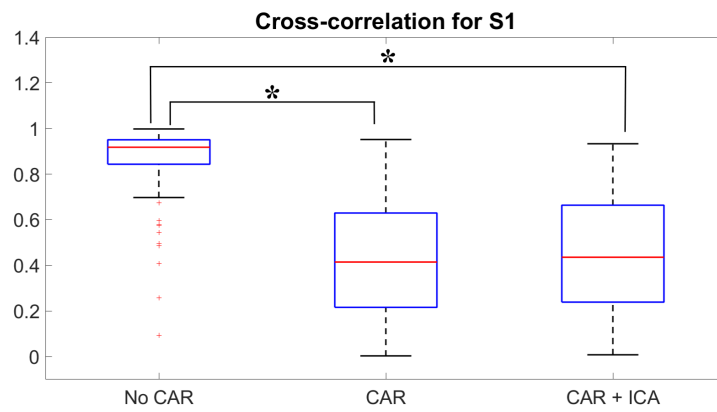
Figure B.1: Cross-correlation results: *Cross-correlation results for **S1**. The asterisks are the results of the ANOVA test (the two groups are statistically different).*
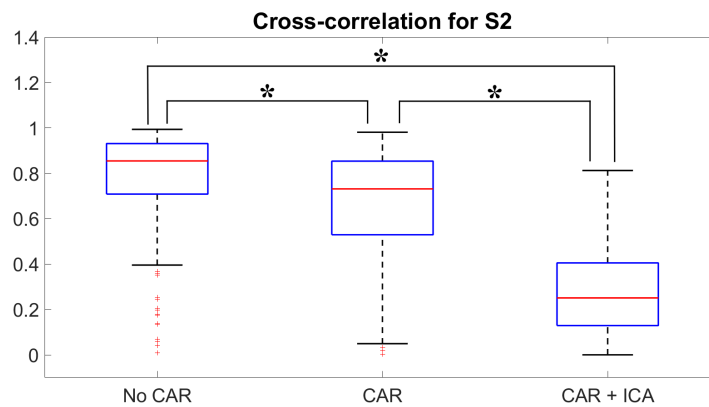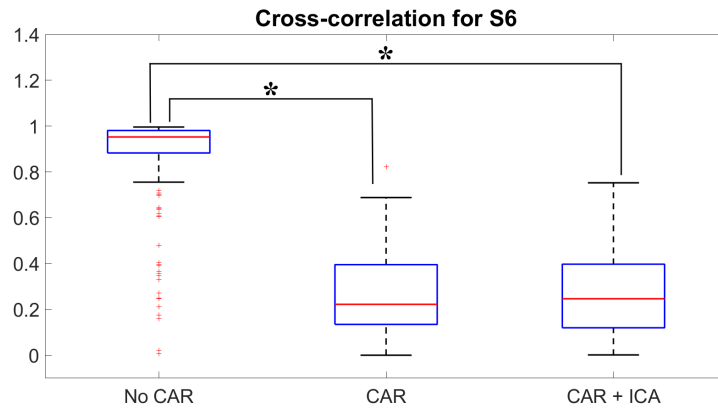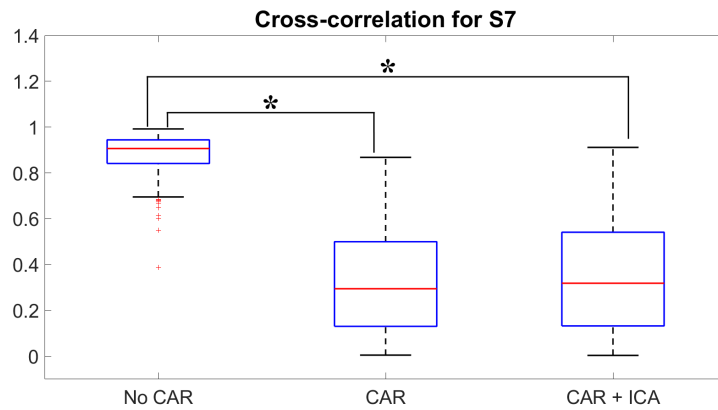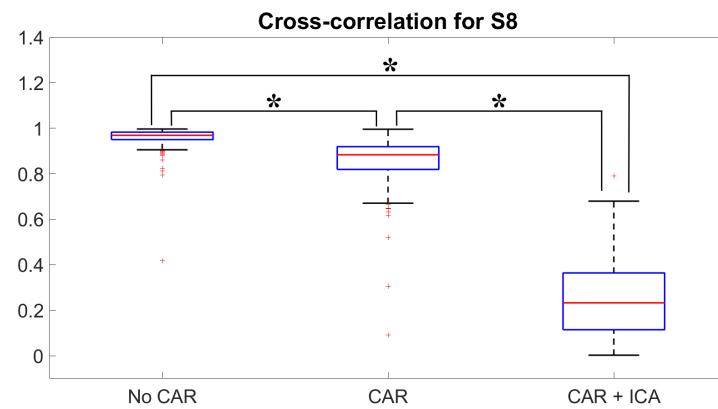

Figure B.2: Cross-correlation results: *Cross-correlation results for **S2**. The asterisks are the results of the ANOVA test (the two groups are statistically different).*
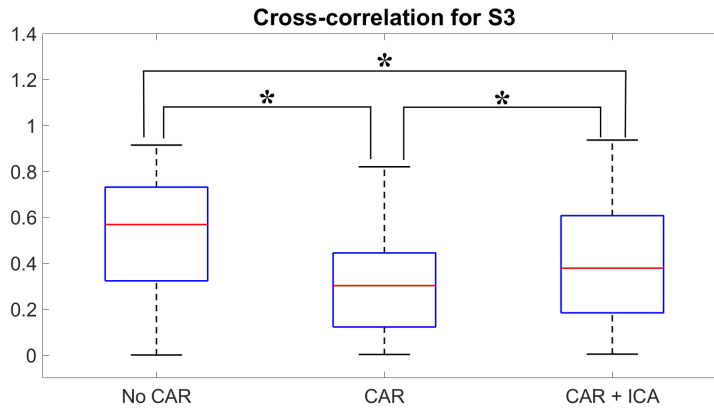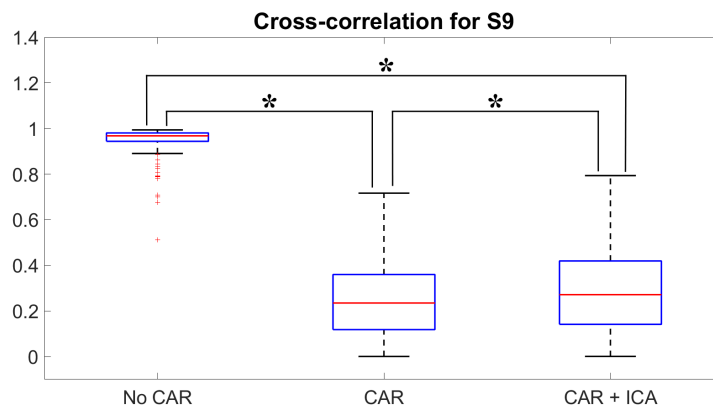
Figure B.3: Cross-correlation results: *Cross-correlation results for **S3**. The asterisks are the results of the ANOVA test (the two groups are statistically different).*
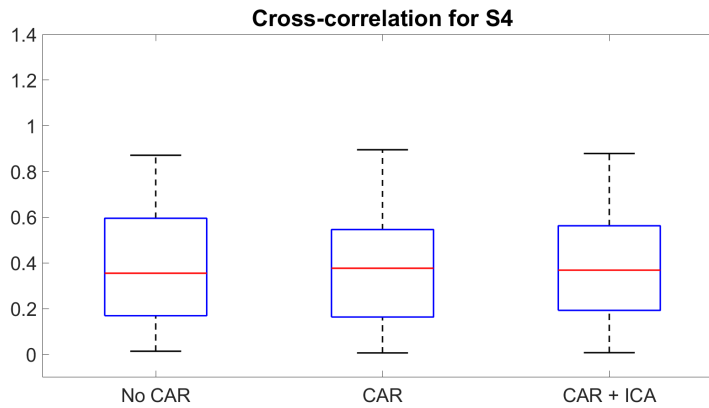
Figure B.4: Cross-correlation results: *Cross-correlation results for **S4**. The asterisks are the results of the ANOVA test (the two groups are statistically different).*
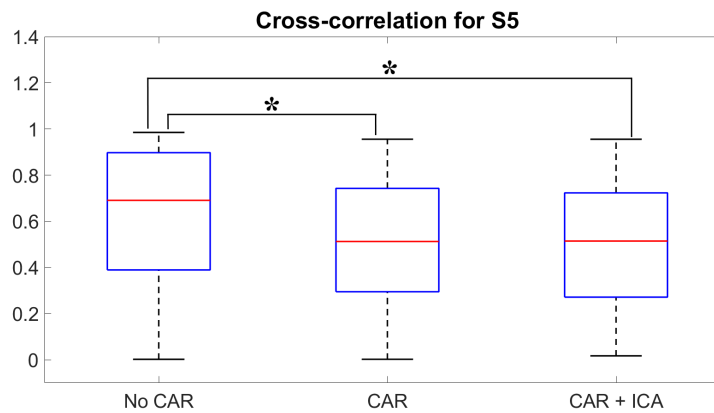
Figure B.5: Cross-correlation results: *Cross-correlation results for **S5**. The asterisks are the results of the ANOVA test (the two groups are statistically different).*

Figure B.6: Cross-correlation results: *Cross-correlation results for **S6**. The asterisks are the results of the ANOVA test (the two groups are statistically different).*

Figure B.7: Cross-correlation results: *Cross-correlation results for **S7**. The asterisks are the results of the ANOVA test (the two groups are statistically different).*

Figure B.8: Cross-correlation results: *Cross-correlation results for **S8**. The asterisks are the results of the ANOVA test (the two groups are statistically different).*

Figure B.9: Cross-correlation results: *Cross-correlation results for **S9**. The asterisks are the results of the ANOVA test (the two groups are statistically different).*

Appendix C

AUC results - sliding window classification
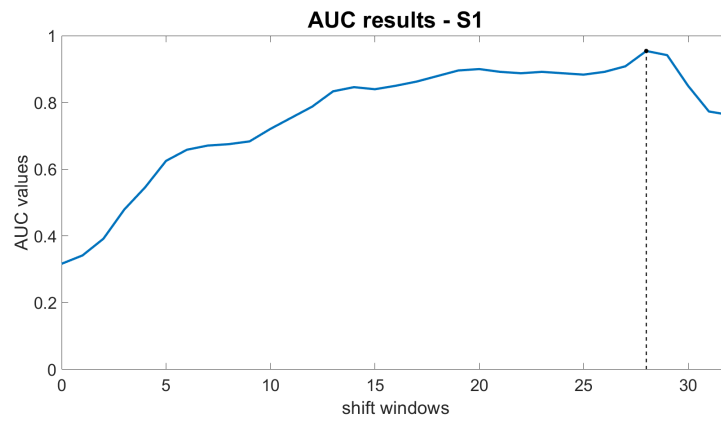
Figure C.1: AUC results*: AUC results for S1. The vertical line represents the highest AUC value*
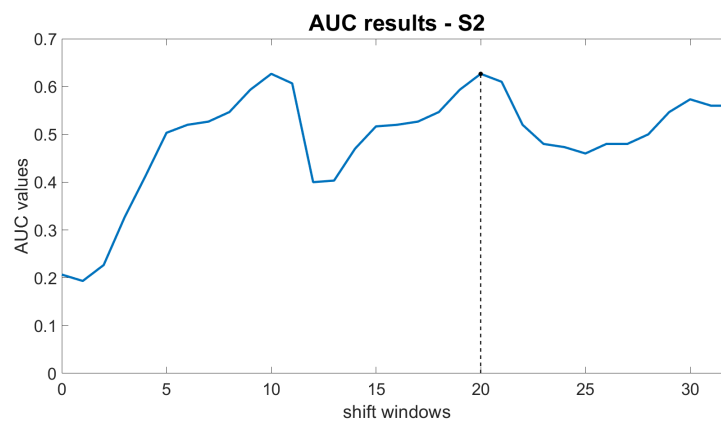
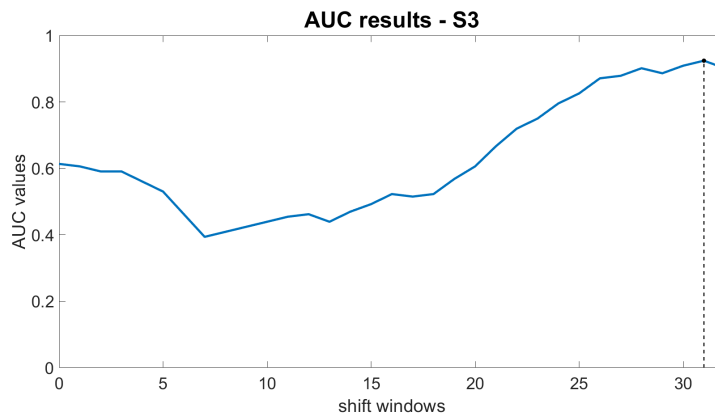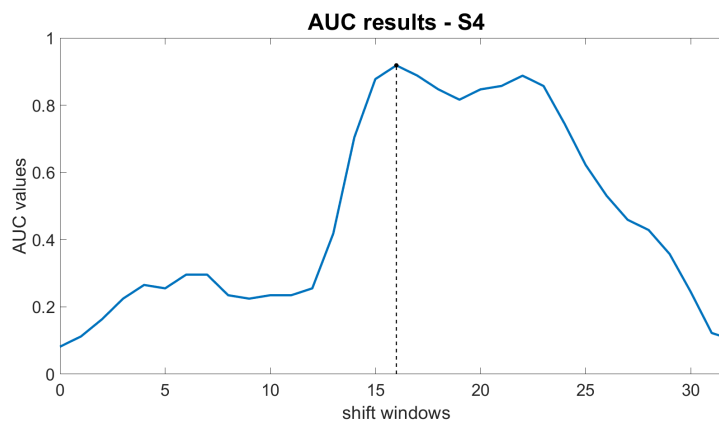***Figure C.2: AUC results****: AUC results for S2. The vertical line represents the highest AUC value*
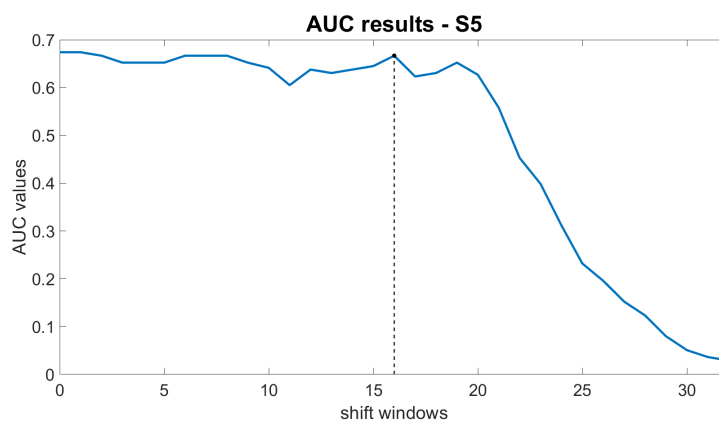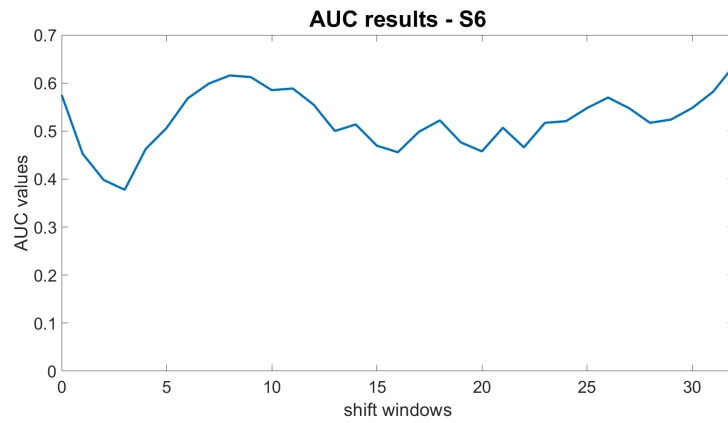
Figure C.3: AUC results*: AUC results for S3. The vertical line represents the highest AUC value*

Figure C.4: AUC results*: AUC results for S4. The vertical line represents the highest AUC value*

Figure C.5: AUC results*: AUC results for S5. The vertical line represents the highest AUC value*

Figure C.6: AUC results*: AUC results for S6. The vertical line represents the highest AUC value*
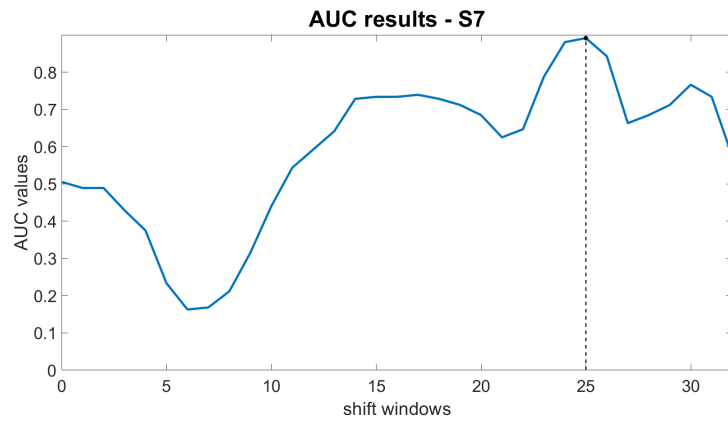

Figure C.7: AUC results*: AUC results for S7. The vertical line represents the highest AUC value*
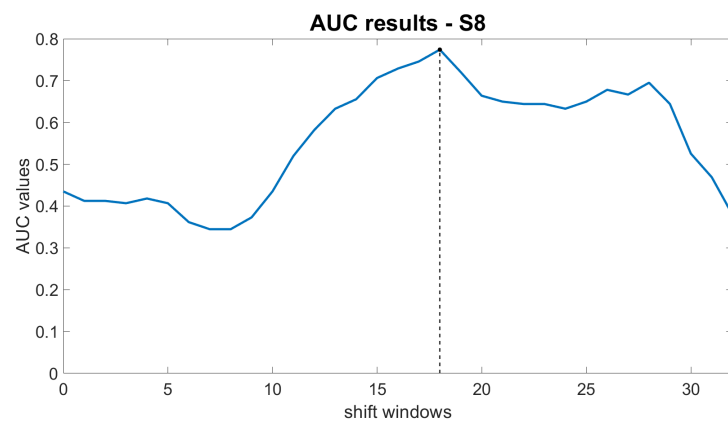

Figure C.8: AUC results*: AUC results for S8. The vertical line represents the highest AUC value*

Figure C.9: AUC results*: AUC results for S9. The vertical line represents the highest AUC value*